HHS Public Access

Author manuscript

Mol Cell. Author manuscript; available in PMC 2020 February 21.

Published in final edited form as:

Mol Cell. 2019 February 21; 73(4): 830–844.e12. doi:10.1016/j.molcel.2018.12.001.

The Functional Proximal Proteome of Oncogenic Ras Includes mTORC2

Joanna R. Kovalski[1,2], **Aparna Bhaduri**[3], **Ashley M. Zehnder**[1], **Poornima H. Neela**[1], **Yonglu Che**[1,2], **Glenn G. Wozniak**[1], and **Paul A. Khavari**[1,2,4,*]

[1]Program in Epithelial Biology, Stanford University, Stanford, CA 94305, USA

[2]Program in Cancer Biology, Stanford University, Stanford, CA 94305, USA

[3]The Eli and Edythe Broad Center for Regeneration Medicine and Stem Cell Research, University of California San Francisco, San Francisco, CA 94131, USA

[4]Lead Contact

SUMMARY

Proximity-dependent biotin labeling (BioID) may identify new targets for cancers driven by difficult-to-drug oncogenes, such as Ras. Therefore, BioID was used with wild-type (WT) and oncogenic mutant (MT) H-, K-, and N-Ras, identifying known interactors, including Raf and PI3K, as well as a common set of 130 novel proteins proximal to all Ras isoforms. A CRISPR screen of these proteins for Ras-dependence identified mTOR, which was also found proximal to MT Ras in human tumors. Oncogenic Ras directly bound two mTOR Complex 2 (mTORC2) components, mTOR and MAPKAP1, to promote mTORC2 kinase activity at the plasma membrane. mTORC2 enabled the Ras pro-proliferative cell cycle transcriptional program and perturbing the Ras-mTORC2 interaction impaired Ras-dependent neoplasia in vivo. Combining proximity-dependent proteomics with CRISPR screening identified a new set of functional Ras-associated proteins, defined mTORC2 as a direct Ras effector, and offers a strategy for finding new proteins that cooperate with dominant oncogenes.

Graphical Abstract

Ras is mutationally activated across many cancers and difficult to target therapeutically. Kovalski et al. identify the functional proximal proteome of oncogenic Ras in cancer, integrating BioID

*Correspondence: khavari@stanford.edu.

AUTHOR CONTRIBUTIONS

J.R.K. conceived the study, designed and executed experiments, analyzed data, and wrote the manuscript. A.B. designed experiments and performed bioinformatic analysis. A.Z., P.H.N., Y.C. and G.G.W. designed and executed experiments. A.B., A.Z., Y.C. and G.G.W. reviewed and edited the manuscript. P.A.K. conceived the study, designed experiments, analyzed data, and wrote the manuscript.

DECLARATION OF INTERESTS

The authors declare no competing interests.

proteomics and CRISPR genetics. They demonstrate that active Ras binds and stimulates mTORC2, representing a key dependency for Ras-driven proliferation genes and tumorigenesis.

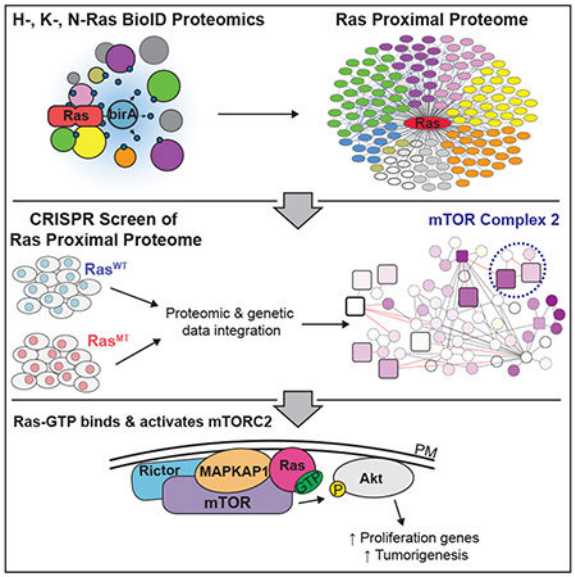

Keywords

Cancer; Ras; Proteomics; CRISPR; mTOR; MAPKAP1

INTRODUCTION

Oncogenic mutations in *KRAS, NRAS* and *HRAS* are present in approximately one-third of all human cancers (Prior et al., 2012). Through the switch between the GTP-bound active and GDP-bound inactive states, the small GTPase Ras proteins transduce extracellular growth signals to downstream effector pathways (Stephen et al., 2014). However, most oncogenic Ras mutants have impaired GTPase function and diminished sensitivity to negative regulators, leading to constitutive activation of pro-neoplastic signaling (Haigis, 2017). Ras is an important clinical target in cancer, however, its structure and complex regulation present challenges to drugging it therapeutically (Papke and Der, 2017).

Defining the spectrum of Ras interacting partners could provide a better understanding of its actions in cancer. Traditional mass spectrometry studies using affinity purification approaches require stable protein interactions in cell extracts (Goldfinger et al., 2007; Shankar et al., 2016). This constraint hinders the capture of transient and dynamic Ras signaling contacts in living cells. Live cell proximity-dependent biotin labeling of proteins (BioID) (Kim and Roux, 2016) may identify new targets for Ras-driven tumors, allowing *in situ* identification of proteins vital for oncogene function that may be missed by conventional approaches. BioID employs a mutant form of the *Escherichia coli* biotin ligase (BirA*) to biotinylate proteins within a ~10nm radius (Roux et al., 2012) and has been applied to a wide array of proteins located in diverse subcellular compartments (Varnaite and

MacNeill, 2016). Therefore, BioID may provide an avenue to identify Ras-proximal proteins in living cells.

Here, we apply BioID to WT and MT H-, K-, and N-Ras isoforms in relevant cancer types where each isoform is mutationally active. The resulting proximal Ras proteome identified known canonical downstream effectors, such as Raf and PI3K, and also found previously unassociated proteins that suggest novel biological actions for Ras. To define which of these newly identified Ras-proximal proteins are functionally relevant, a CRISPR-based screen was performed in a series of Ras isoform-dependent and independent cancer cells as well as in non-transformed cells. Integration of proteomics and CRISPR data sets identified mTOR as the top newly identified protein proximal to Ras that was also required for cancer cell growth driven by oncogenic Ras. The majority of prior work suggests mTOR is not regulated by Ras through direct contact, but rather distally via Ras stimulation of the PI3K and the MAPK pathways (Kim et al., 2016). However, direct association of Ras with mTOR Complex 2 (mTORC2) component MAPKAP1 and between their homologs in a model organism have prompted speculation that Ras may regulate mTORC2, although with no known mechanism in cancer (Guertin and Sabatini, 2007; Schroder et al., 2007; Yao et al., 2017). We demonstrate that GTP-loaded Ras interacted directly and selectively with mTORC2 through two distinct interactions: binding MAPKAP1, consistent with previous data, but also direct association with the mTOR kinase domain via the Ras effector binding domain. Active Ras increased mTORC2 enzymatic activity *in vitro* and in cells at the plasma membrane to positively co-regulate cell cycle genes. Disruption of MT Ras and mTORC2 proximity decreased mTORC2 phosphorylation activity, transcriptional dysregulation, and reduced Ras-driven in vivo tumorigenesis. Taken together, these data suggest that mutant Ras acts, in part, through direct interaction with mTOR to promote mTORC2 activity in cancer.

RESULTS

Proximal Proteins to Ras Isoforms in Cancer Cells

The proximal Ras proteome in cancer may include new therapeutic targets, thus, we performed BioID with WT and MT H-, K-, and N-Ras isoforms (Figure 1A). The BioID experiments were carried out in cancer cell types where each Ras isoform is commonly mutated (Prior et al., 2012), but in cell lines that are Ras wild-type to enable isogenic comparison of the WT and MT proteomic datasets. Bladder cancer cells were used for H-Ras, colon cancer cells were used for K-Ras, and melanoma cells were used for N-Ras. The specific mutant alleles chosen for each Ras isoform were the most prevalent mutation for the corresponding cancer type in the COSMIC database. BirA*-Ras fusions were expressed at 0.25- to 5-fold the level of the endogenous isoform (Figures S1A-B) and were able to activate downstream pathways (Figures S1C-D), promote cell growth (Figure S1E) and localize to the membrane fraction of the cell (Figure S1F), reflecting native Ras subcellular distribution (Hernandez-Valladares and Prior, 2015). BirA*-Ras fusion proteins thus recapitulate the actions of unfused Ras isoforms.

To identify Ras-proximal proteins in living cells, biotin was added to birA*:Ras and birA* control cells followed by streptavidin pulldown and validation of known Ras interactors. The

small amount of biotin present in the cell culture media enabled some basal biotinylation of high affinity Ras interactors, such as Raf1, however, 24 hours of biotin labeling demonstrated maximal biotinylation signal, consistent with the published BioID protocol (Roux et al., 2013) (Figures S1G-H). Following mass spectrometry analysis, the resulting data were thresholded for minimum spectral count and fold change over control as well as filtered via Significance Analysis of INTeractome (SAINT), which uses a probability model to assign a confidence score to each interaction (Choi et al., 2011). The analysis identified 690 proteins proximal to at least one Ras isoform (Figure 1B**;** Table S1), increasing the number of potential Ras-proximal proteins by an order of magnitude.

The Ras-proximal proteome included many canonical Ras interacting proteins, providing support for the validity of this dataset. The network of proteins interacting replicably with at least one Ras isoform included receptors such as EGFR, regulators of Ras activity such as NF1, and downstream Ras effectors such as Raf and PI3K proteins (Figure S2A). The absence of some canonical Ras interactors, such as RalGDS, may be due to the known inability of BioID technology to equally biotinylate all proteins, as a surface and accessible lysine on proximal proteins is required. Analysis of the relative RNA expression for the proteins identified within a single Ras isoform interactome suggested that isoform specificity was not only a reflection of cell type expression, thereby highlighting possible candidates for future studies of isoform-specific therapeutic targets (Figure S2B). BioID can thus be used to identify new proteins proximal to highly dynamic signaling proteins, such as Ras, in a relevant cancer cell context.

Of the 690 total Ras-proximal proteins identified, 150 were common to all Ras isoforms in all cell types examined (Figure 1C). This common set of 150 proteins were highly enriched ($p < 1\times10^{-10}$) for known protein-protein interactions among themselves, suggesting capture of biologically relevant signaling and regulatory modules. Of the 150 common proximal Ras proteins 42, favored oncogenic Ras with an average 2-fold greater peptide spectral count in the mutant compared to WT Ras data (Table S1). The majority of these 150 proteins have never been previously linked to Ras directly or to a Ras pathway (Figure 1D), consistent with the limited number of published Ras proteomic studies. Spectral count distributions between known Ras interactors and the novel 130 proximal proteins were similar, supporting these new candidates as real signal and not experimental noise (Figure S2C-D). Importantly, the common group of 150 Ras proximal proteins was statistically enriched for well-known Ras cellular functions, such as cytoskeleton and cell junction integrity (Karnoub and Weinberg, 2008) (Figure S2E-F). Further validating Ras adjacency to the proteins identified, the proximity ligation assay (PLA), which detects endogenous proteins within 30-40nM to produce a fluorescent signal, corroborated endogenous Ras co-localization with series of select candidates in intact cells at a level similar to Ras interaction with Raf1 (Figures 1E-F **and** Figures S2G-I). Unexpectedly, a group of small molecule transporters was also found proximal to Ras. The common set of Ras-proximal proteins thus includes both known and novel Ras protein associations.

CRISPR Screen to Distil a Functional Set of Ras-Proximal Proteins

To distil proteins that are functionally required for Ras-driven cancer growth from the identified set of Ras-proximal proteins, CRISPR-based knockout screening was performed. This approach provides a way to isolate genes contributing to a phenotype of interest, in this case the growth of Ras-dependent tumor cells. The 150 common Ras-proximal proteins were targeted in 5 cancer lines whose growth is dependent on oncogenic MT Ras isoforms and 4 cancer lines independent of Ras. To distinguish genes that are generally required for cell viability, non-transformed, diploid primary human cells were also screened, bringing the total number of cell types to 10. The CRISPR screen achieved high global coverage of unique guides and demonstrated the expected changes when targeting control genes and appropriate dependency on the relevant MT Ras isoform (Figure S3A-E**;** Table S2). Additionally, in support of the differential MT and WT Ras BioID proteomes, genetic loss of proteins proximal to MT Ras was more deleterious than was loss of proteins proximal to WT Ras isoforms (Figure S3F). 17 novel Ras-proximal proteins that negatively impact proliferation of cancer cells dependent on oncogenic Ras (Figure 2A**;** Table S3) were identified using MAGeCK statistical analysis (Li et al., 2014). These proteins represent newly identified proteins proximal to oncogenic Ras that are also required for growth of Ras-driven cancer cells.

To search for new protein subnetworks most critical to oncogenic Ras function, the BioID proteomics and CRISPR genetic screen data were further integrated. The 17 candidates were pared down to 5 with both known protein-protein interactions within the common Ras proximal proteome and a significantly deleterious impact on multiple Ras-dependent cell lines. The protein interaction network built by connecting these 5 proteins with other common proximal Ras proteins, highlighted known functional subnetworks for Ras, such as PI3K and Raf signaling, and adhesion (Pylayeva-Gupta et al., 2011) (Figure 2B). A subnetwork anchored by mTOR, was the most highly ranked to favor oncogenic MT Ras over WT Ras in the integrative genetic and proteomic analysis across all three isoforms and multiple cell types. This highlighted the existence of an underappreciated physical proximity relationship between Ras and critical tumorigenic signaling mediated by mTOR.

mTOR Interacts with Oncogenic Ras

mTOR is a master regulator of core oncogenic processes, such as dysregulated cell proliferation, improved cell survival, and metabolic alterations (Laplante and Sabatini, 2012). First, MT Ras-mTOR proximity was confirmed by BioID-western blot, which detected robust mTOR proximity to MT Ras over WT Ras isoforms (Figure S4A). Addition of excess biotin did not appear to impact mTORC2 activity (Figure S4B-C). Ras and mTOR co-localization was further validated by PLA analysis of endogenous proteins in *NRAS, HRAS* and *KRAS* wild-type and mutant cancer cells with increased signal observed in the MT Ras lines (Figure 2C-D; S4D-G). To further support the selective association of MT Ras with mTOR, co-immunoprecipitation (co-IP) of a HA-tagged $NRAS^{WT}$ or $NRAS^{Q61K}$ was performed in WT melanoma cells. N-Ras bound endogenous mTOR with preference for active MT N-Ras similar to canonical Ras effectors p110α and Raf1 (Figures 2E-F). Likewise, pulldown of HA-tagged $NRAS^{Q61K}$ co-immunoprecipitated endogenous mTOR, p110α, and Raf1 in two oncogenic NRAS melanoma cell lines (Figures S4H-I). PLA

analysis of the association of MT Ras with mTOR in *KRAS* genotyped human colon adenocarcinoma specimens demonstrated enhanced Ras-mTOR signal in *KRAS* MT over WT tumors to a similar extent as positive control Ras-Raf1 (Figure 2G-H**;** S4J-L). Thus, endogenous Ras-mTOR proximity is present in human cancer cell lines and tissue specimens, further confirming the preference for Ras in the GTP-bound state.

To study the direct physical association between Ras and mTOR, we employed a series of biochemical assays on purified proteins. First, far western-blotting with recombinant proteins for all 3 Ras isoforms was performed, to further assess the ability of GTPγS-bound MT and GDP-bound WT Ras to associate with mTOR. To a varying degree across Ras isoforms, purified recombinant mTOR bound MT Ras to a greater extent than WT Ras (Figure S4M-N) and within the range of canonical Ras effectors-Raf1, PI3K and RalGDS (Figure S4O-P). Second, crosslinking mass spectrometry (XL-MS) analysis of GTP-bound N-Ras^{Q61K} with mTOR identified a number of high confidence crosslinks between N-Ras residues structurally proximal to the Switch I and II regions and the mTOR kinase domain (Figure S4Q), suggesting a model similar to the well-established Rheb GTPase interaction with mTORC1 (Long et al., 2005). Interestingly, the XL-MS analysis also highlighted a number of interactions between Ras and mTOR HEAT repeats, which is consistent with the secondary region Rheb binds in a co-crystal structure with mTORC1 (Yang et al., 2017). Finally, Microscale Thermophoresis (MST) was used to address the Ras and mTOR interaction in a quantitative manner where both proteins are free in solution. Positive control Raf1^{RBD} demonstrated a clear preference for Ras-GTP as compared to Ras-GDP (Figure 2I and Figure S4R) with a dissociation constant (K_d) in line with published studies (Sydor et al., 1998). Based on the Rheb-mTORC1 interaction model and the XL-MS data above, the mTOR kinase domain was assayed for binding to Ras-GTP or Ras-GDP. Ras-GTP bound the mTOR kinase domain with increased affinity over Ras-GDP (Figure 2J) with a comparable K_d to two other established Ras effector proteins, PI3Kγ and RalGDS (Pacold et al., 2000), with a nucleotide state-dependent K_d shift similar to other small GTPases that bind mTOR (Long et al., 2005; Tatebe et al., 2010). An mTOR HEAT region, containing repeats 1-9, to exclude the majority of XL-MS links, displayed a lower affinity for Ras-GTP. These data support a direct interaction between active Ras-GTP and the mTOR kinase domain.

Oncogenic Ras Associates with mTORC2 via the Ras Effector Binding Domain

mTOR operates within at least two distinct functional complexes, mTORC1 and mTORC2. While Ras impacts downstream mTOR activity in the context of mTORC1 through both MAPK-and PI3K-mediated inactivation of the negative mTORCI regulator TSC1/2 (Kim et al., 2016), the relationship of Ras to mTORC2 in cancer has been less understood beyond its link to MAPKAP1. Integrative analysis of proteomics and CRISPR data identified no mTORC1-specific proteins, however, it found two key mTORC2 components, Rictor and MAPKAP1. The CRISPR screen identified the necessity for *MAPKAP1* in Ras-dependent cancer lines, yet unexpectedly, there was no deleterious impact with loss of *RICTOR,* which likely reflects suboptimal targeting guide design. To further bolster a MT Ras dependency on *RICTOR,* we performed an independent analysis of 341 cell lines across 19 cancer types in the Project Achilles CRISPR screen database, identifying a significant positive correlation between *HRAS* and *RICTOR* (p-value = 0.025). The Ras BioID proteomics data as well as

our, and publicly available, CRISPR screen data thus point to oncogenic Ras cancer cell dependency on mTORC2.

We next sought to experimentally corroborate mTORC2 proximity to oncogenic Ras. BioID-western blotting confirmed MT Ras proximity to mTORC2 via detection of Rictor and MAPKAP1, but not to mTORC1, as assessed by Raptor signal (Figure S5A). Additionally, knockdown of *RICTOR* and *MAPKAP1,* but not *RPTOR,* in birA*:NRAS^{Q61K} expressing melanoma cells decreased the Ras-mTOR proximity signal in BioID pulldown without any consistent impact on Raf1 or p110α (Figure 3A-3C**;** S5B). PLA also supported the selectivity of endogenous MT Ras for mTORC2, and not mTORC1 (Figure S5C-H) and depletion of mTORC2 components, but not mTORC1, decreased endogenous mTOR-Ras PLA signal (Figure 3D-F**;** S5I). Finally, co-IP of HA-tagged WT or MT N-Ras with endogenous mTORC1 or 2 components in WT Ras cells demonstrated a significant increase in MT N-Ras signal only for the mTORC2 components, Rictor and MAPKAP1 (Figure 3G-H). Similar results were observed with the co-IP of HA-tagged NRAS^{Q61K} with endogenous mTORC2 components in MT NRAS melanoma cell lines (Figures S5J-K). Taken together, these data indicate that the binding of oncogenic Ras to mTOR occurs selectively in the context of the mTORC2 complex, and not mTORC1.

To further study the Ras-mTORC2 association, we next examined the residues of Ras required for mTOR proximity. Ras binds effectors via residues adjacent to its Switch I region (Khosravi-Far et al., 1996). Therefore, mutations within the Ras effector domain were used to assess the residues required for active Ras proximity to mTORC2 (Figure S5L). Alanine substitutions in the Ras effector domain affected Ras adjacency to mTOR, MAPKAP1, and Rictor, with T35A and Y40A decreasing it and E37A increasing it (Figure 3I-J). Additionally, T35A and Y40A decreased signaling downstream of mTORC2 where as E37A did not, as indicated by pAKT^{S473} (Sarbassov et al., 2005) and pNDRG1^{T346} levels, an SGK1 target (Garcia-Martinez and Alessi, 2008; Heikamp et al., 2014) (Figures S5M-N). These data indicate that Ras interaction with mTORC2 depends on specific amino acids within the Ras effector interaction domain.

Oncogenic Ras Regulates mTORC2 Activity

Ras regulates the activity of multiple kinases, suggesting that it might also impact mTORC2 enzymatic function. Moreover, the XL-MS and MST data demonstrate that Ras binds the kinase domain of mTOR, therefore, mTORC2 enzymatic activity was assessed as a function of active Ras. First, cellular co-expression of NRAS^{Q61K}, but not wild-type NRAS or RHEB, increased mTORC2 kinase activity towards a GST-Akt1 tail substrate *in vitro,* an increase which could be reversed by addition of an mTOR inhibitor (Figure 4A-B). Second, addition of purified recombinant Ras^{G12V}-GTPγS to mTORC2 promoted its activity, in contrast to addition of GDP-bound Ras^{WT}, which did not (Figure 4C**;** S6A). The modest, yet significant increase in mTORC2 kinase activity with the addition of Ras-GTP is concordant with the reported impact of Ras-GTP on Raf1 and PI3K kinase activity in vitro (Rodriguez-Viciana et al., 1996; Stokoe and McCormick, 1997). Therefore, GTP-bound MT Ras increases the kinase activity of mTORC2.

Although the *in vitro* kinase assay provides a direct assessment of the influence of Ras on mTORC2, it cannot provide information on where in the cell this vital interaction and functional impact occurs. We examined subcellular mTORC2 kinase function in intact cells with the LocaTOR2 assay (Ebner et al., 2017), which uses the mTORC2 substrate, Akt, to measure mTORC2 phosphorylation activity at specific subcellular locations (Figure 4D). To quantify the mTORC2 activity in a specific subcellular compartment, the phosphorylated Frb:Akt band was normalized to its total Frb:Akt signal then normalized to the baseline no drug signal. In MT *NRAS* melanoma cells, mTORC2 activity was chiefly localized to the plasma membrane, but also the late endosome and mitochondria; this activity could be suppressed by pan-mTOR inhibition (**Figures** 4E**;** S6B). Knockdown of MT *NRAS* resulted in a specific decrease in mTORC2 kinase activity at the plasma membrane but not at the other main sites (**Figures** 4F-G**;** S6C). Thus, oncogenic Ras enables mTORC2's activity at the plasma membrane.

MAPKAP1 Binds Ras and Modulates the Ras-mTORC2 Interaction

The finding that MT Ras enables mTORC2 activity at the plasma membrane prompted examination of membrane-associating mTORC2 components. MAPKAP1 is a key mediator of mTORC2 membrane association through the lipid binding capacity of its pleckstrin homology domain (Liu et al., 2015) and can bind Ras *in vitro* via a potential Ras binding domain (RBD) (Schroder et al., 2007) (Figure 5A). The dependency of mutant Ras cells on *MAPKAP1,* as identified in the CRISPR screen, was confirmed by the significant reduction in cell division upon *MAPKAP1* depletion (Figure S6D-E). We next sought to validate if MAPKAP1, similar to mTOR, also binds Ras-GTP. Far western-blotting with purified recombinant proteins supported the Ras-MAPKAP1 association (Figure S4O-P). To more precisely isolate the region of interaction between Ras and MAPKAP1, N-Ras^{Q61K} and MAPKAP1 were subjected to XL-MS analysis. The only high confidence inter-protein contacts occurred between the proposed MAPKAP1 RBD at K310 and K317 and N-Ras residues structurally proximal to the Switch I and II regions. (Figure S6F). In MST experiments, purified recombinant WT MAPKAP1^{RBD} (Figure S4R) bound Ras-GTP with an order of magnitude increase compared to Ras-GDP (Fig. 5B). Mutation of three key residues in the MAPKAP1 RBD, homologous to critical Raf1 RBD positions (Barnard et al., 1995) and overlapping with the XL-MS crosslinks, decreased MAPKAP1^{RBD} interaction with Ras-GTP 10-fold (Figure S6G). Taken together, these data indicate that active Ras-GTP can directly associate with both mTOR as well as MAPKAP1 and also suggest that altering MAPKAP1 protein function might decouple mTORC2 and oncogenic Ras.

To do this, we generated a reagent to disrupt the mTORC2-Ras interaction without mTORC2 complex dissolution. Previous publications identified a minimal N-terminal mTORC2 binding region on MAPKAP1 (Cameron et al., 2011) (Figure 5A). Deleting the C-terminal region of MAPKAP1 (MAPKAP1^{Del}) produced an intact mTORC2 that lacked the RBD and membrane localization capability (Figure S6H). MAPKAP1^{Del}, by blocking mTORC2 localization to the plasma membrane and its association there with Ras, would be predicted to act in a dominant-negative manner to inhibit Ras-mTORC2 interaction. Consistent with this, MAPKAP1^{Del} expression decreased MT Ras proximity to both mTOR and Rictor without affecting Ras interactions with either Raf1 or PI3K (Figure 5C-D).

Additionally, MAPKAP1^{Del} expression diminished the PLA signal of endogenous Ras with both mTOR and Rictor in MT *NRAS* melanoma cells, whereas, full length MAPKAP1^{WT} did not (Figure 5E-F). Moreover, MAPKAP1^{Del} specifically inhibited mTORC2 activity at the plasma membrane in the LocaTOR2 assay (Figure 5G-H**;** S6I). Therefore, mTORC2 requires full length MAPKAP1 for both interaction with Ras and for Ras-enabled mTORC2 enzymatic function, and a MAPKAP1^{Del} mutant lacking an RBD and membrane localizing sequences acts dominantly to disrupt these processes.

mTORC2 is Required for Ras Cell Cycle Gene Regulation

The observation that MT Ras binds and enables mTORC2 activity suggested that mTORC2 might enable Ras impacts in cancer, prominent among which are downstream gene regulation (Pylayeva-Gupta et al., 2011). A requirement for mTORC2 in oncogenic Ras target gene induction was therefore examined. To obtain baseline signatures in normal diploid cells, and as a comparator to *NRAS* mutant melanoma cells, primary non-transformed human melanocytes were used to distill mTORC1 versus mTORC2-dependent genes by RNA-sequencing (Figure S7A**;** **Tables** S5–6). In these cells, only loss of *RICTOR,* but not *RPTOR,* correlated with a significant shift towards gene expression seen in WT *NRAS* patient melanoma specimens from TCGA data (Figure 6A), suggesting that intact mTORC2 mediates a portion of the MT Ras gene expression program in melanoma. Given the direct mTORC2 interaction with MT Ras, the transcriptional consequence of mTORC1 versus mTORC2 loss in an oncogenic Ras-driven cancer cell context was next examined. *RPTOR, RICTOR, MAPKAP1* or *NRAS* were depleted in duplicate in independent *NRAS* MT melanoma lines followed by RNA-sequencing (Figure 6B**;** S7B-S7F). The gene signature downregulated with loss of both oncogenic *NRAS* and mTORC2 components was enriched for cell proliferation gene ontology (GO) terms compared to genes co-dependent on MT *NRAS* and mTORC1 with expression of select genes validated by qPCR (Figure 6C-D**;** S7G-I). Consistent with a cell cycle regulatory function, the mTORC2 and MT *NRAS* gene signature was also enriched for binding by E2F family transcription factors (Figure S7J-K) (Dimova and Dyson, 2005). Given the common core motif shared by E2F transcription factions, as in the HOCOMOCO database, however, a specific E2F family could not be identified. Overall, this genetic perturbation analysis suggests that mTORC2 enables the pro-proliferative cell cycle transcriptional program driven by oncogenic Ras.

To extend the transcriptional signature analysis to patient specimens, GSEA was used to identify pathways positively co-enriched with higher *MTOR, RICTOR* and *MAPKAP1* RNA expression levels in a TCGA *NRAS* mutant melanoma patient cohort. Higher mTORC2 gene expression was positively correlated with cell cycle pathways, in contrast to the predominance of metabolic pathways observed in the overlap of unique *MTOR* and *RPTOR* enriched signatures (Figure 6E). Additionally, pathway interaction database (PID) signatures positively co-enriched with higher mTORC2 gene expression included not only the FOXO pathway, as expected (Oh and Jacinto, 2011), but also the E2F pathway (Figure 6F). Both experimental mTORC2 loss and co-enrichment expression analysis in mutant *NRAS* patient data suggest a critical, yet underappreciated, role for oncogenic Ras and mTORC2 cooperating to positively co-regulate proliferation genes.

Alteration of MAPKAP1 Impedes the Ras-driven Transcriptional Program

To probe the transcriptional impact of physically decoupling oncogenic Ras and mTORC2 without complete mTORC2 disassembly, the functionally dominant negative MAPKAP1^{Del} was expressed in both *NRAS* MT and WT melanoma cells followed by RNA-sequencing. Cell cycle and DNA replication pathways were de-enriched in *NRAS* MT melanoma cells with MAPKAP1^{Del} expression compared to *NRAS* WT cells (Figure 7A**;** Table S6). Moreover, MAPKAP1^{Del} expression in *NRAS* MT melanoma cells recapitulated transcriptional signatures characteristic of *NRAS* WT patient melanomas (Figure 7B**;** Table S6). These data are consistent with a model in which MT Ras exerts a segment of its pro-proliferation transcriptional effects via induction of mTORC2 activity.

Disruption of mTORC2 and Mutant Ras Proximity Impedes Ras-driven Tumorigenesis

If MT Ras interaction with mTORC2 promotes cell proliferation, then its disruption should impair Ras-driven tumor growth. Consistent with this hypothesis, MAPKAP1^{Del}, but not MAPKAP1^{WT}, diminished tumorigenesis of oncogenic *NRAS*-driven MM485 and SK-MEL-2 melanoma cells *in vivo,* but not of WT *NRAS* CHL-1 cells (**Figures** 7C-D**;** S7L-M). MAPKAP1^{Del} also impeded *in vivo* tumorigenesis driven by oncogenic *HRAS* in bladder carcinoma cells and *KRAS* in isogenic colorectal adenocarcinoma cancer lines (Figure S7N-O). Thus, disrupting mTORC2 association with Ras selectively impairs oncogenic Ras-driven tumorigenesis.

Given the demonstrated role of oncogenic Ras on mTORC2 enzymatic activity, MT Ras-driven tumors were assayed for alterations in mTORC2 activity as judged by phosphorylation of direct and downstream pathway substrates. In MT *NRAS* melanoma tumors, MAPKAP1^{Del} expression decreased phosphorylation of the direct mTORC2 target, pAKT^{S473}, as well as SGK1 target pNDRG1, without altering mTORC1 phosphorylation of p4EBP1$^{T37/46}$ or pS6K^{T389}, MAPK activity on pMEK$^{S217/221}$, or PI3K activity on pAKT^{T308} (**Figures** 7E-F**;** S7P-Q). These findings are consistent with an impact specific to mTORC2 without altering other related pathways. Oncogenic Ras association with mTORC2 therefore enables Ras-driven *in vivo* tumor growth, and disrupting Ras-mTORC2 association diminishes tumorigenesis and measures of mTORC2 kinase activity.

DISCUSSION

Here, we identify a core set of 150 proteins proximal to Ras isoforms, using live cell proximity proteomics, to characterize a role for mTORC2 in enabling Ras-driven tumorigenesis. Integration of proximity proteomics with CRISPR screening of oncogenic Ras-dependent cells identified mTORC2 and also detected novel classes of Ras-proximal proteins. The common and isoform-specific Ras-proximal proteins identified here provide a resource for future mechanistic studies. Of particular note are the numerous Ras-proximal small molecule transporters, including the CRISPR screen hits *SLC7A5* and *SLC3A2,* which form a functional heteromeric amino acid transporter and can regulate integrin signaling in an oncogenic Ras context (Estrach et al., 2014). This protein family may represent an as yet unexploited modality to disrupt core oncogenic Ras function. Additionally, the isoform-specific Ras-proximal proteins provide insight into isoform unique

functions and protein partners. Future studies with these candidates may expand insight into how each isoform drives different cancer types as has been partially described for K-Ras (Wang et al., 2015). Previous studies have separately used BioID proteomics to highlight oncogenic interactors or employed CRISPR genetics to screen for oncogene dependency (Dingar et al., 2015; Wang et al., 2017). However, the serial integration of both approaches filtered through specific cell dependency phenotypes, in this case for oncogenic Ras, may increase available therapeutic options for difficult-to-drug oncogenes.

The robustness of the integrated proteomic and genetic screening approach used here is supported by strong corroborating biochemical and biophysical evidence of a direct binding relationship between MT Ras and mTORC2. Proximity proteomics demonstrated MT Ras proximity to mTORC2 with CRISPR genetics supporting a MT Ras dependency on both mTOR and MAPKAP1. Critically, functional analyses with MST, co-immunoprecipitation and far western data substantially support a direct physical association of oncogenic Ras with mTOR and MAPKAP1, with interaction constants consistent with canonical Ras effectors. Furthermore, we demonstrate the ability of active Ras to promote the kinase activity of mTORC2 both *in vitro* and within live cells. All together the data implicate mTORC2 as a bona fide, direct Ras effector required for oncogenic Ras-driven pro-proliferative gene expression and tumorigenesis.

The data demonstrating active Ras binding to mTORC2 with two distinct points of contact suggest new hypotheses. The previously observed dimerization of Ras in live cells supports a model with two Ras molecules bind to mTORC2 simultaneously (Nan et al., 2015). The comparatively high dissociation constant detected for the mTOR kinase domain with Ras-GTP as compared with MAPKAP1 RBD suggests that MAPKAP1 might serve as a high affinity adapter protein to recruit active Ras to the complex to facilitate Ras promotion of mTORC2 kinase activity. Indeed, the high affinity Ras-MAPKAP1 interaction leaves open the possibility that MAPKAP1 may have Ras-related functions outside of mTORC2. However, evidence from lower organisms, emphasizes the pervasiveness of small GTPases binding directly to and modulating mTOR enzymatic activity, subcellular localization, and substrate recruitment (Khanna et al., 2016; Long et al., 2005; Tatebe et al., 2010). Moreover, examination of well-established Ras biology highlights a parallel between the structurally homologous mTOR and PI3K p110 kinase domains, wherein Ras association with PI3KY causes a structural change to affect PI3K catalytic activity (Walker et al., 1999). Our data support a similar model for Ras and mTOR in the context of mTORC2. Further structural studies are warranted to decipher the precise nature of Ras association with mTORC2.

Our protein-protein interaction network derived from the integrative analysis of the proteomic and genetic screen datasets highlights Ras-mTORC2 association as a potential therapeutic target. Moreover, the selective, negative impact of disrupting the Ras-mTORC2 interaction on Ras-driven cancers provides mechanistic insight into the potential requirement for mTORC2 in Ras-driven pancreatic tumorigenesis (Driscoll et al., 2016) and the clinical efficacy of combining PI3K/mTOR and MAPK inhibitors in oncogenic Ras-driven neoplasias (Gysin et al., 2011). A recent study screened for small moleucles to uniquely target mTORC2, suggesting direct inhibition is a feasbile pharmacological goal (Benavides-Serrato et al., 2017). The identification of Ras interaction with mTORC2 further supports the

rationale to develop mTORC2-specific inhibitors for the treatment of cancers driven by oncogenic Ras as well as the exploration of additional nodes in the identified Ras proximal protein network for future therapeutic opportunities.

STAR METHODS

CONTACT FOR REAGENT AND RESOURCE SHARING

Further information and requests for resources and reagents should be directed to and will be fulfilled by the Lead Contact, Paul Khavari (khavari@stanford.edu).

EXPERIMENTAL MODEL AND SUBJECT DETAILS

Animals—8-week old, female SHO mice (Crl:SHO-*Prkdc*^{scid}*Hr*^{hr}) were purchase from Charles River. Animal cohort numbers were chosen based on results from tumorigenesis pilot studies in mice. Animals were randomly assigned to experimental groups. Animals were not involved in any previous procedures prior to subcutaneous tumor injection. Researchers were not blinded to experimental group identity. Mice were housed five to cage with autoclaved bedding, food and water. All animals under assessment were weighed at least once a week to observe any changes indicative of poor health status. All the study procedures related to mouse handling, care, and assessment were performed according to the guidelines approved by the Stanford University Administrative Panel on Laboratory Animal Care (APLAC).

Human Specimens—Colon Adenocarcinoma specimens with known *KRAS* and *BRAF* mutation status were procured from Asterand Biosciences (Bipoint). The samples were collected under IRB approved protocols with informed consent. The samples are deidentified to ensure patient confidentiality.

Cell Lines and Primary Cells—All cell lines and primary cells were cultured at 37 °C, 5% CO2. HEK-293T, SK-MEL-5 and CHL-1 were cultured on DMEM 10% FBS, 1% Pen-Strep; HT-1376, Caco-2, SK-MEL-2 and LS174T were cultured in EMEM 20% FBS, 1% Pen-Strep; BxPC-3, MM415, MM485, AsPC-1, DLD-1 KRAS$^{WT/-}$, and DLD-1 KRAS$^{G13D/-}$ were cultured in RMPI-1460 (ATCC Modification) 10% FBS, 1% Pen-Strep; T24 and Capan-2 were cultured in McCoy's 5A (Modified) 10% FBS, 1% Pen-Strep. CHL-1, HT-1376, Caco-2, Capan-2, SK-MEL-2, SK-MEL-5, LS174T, AsPC1 and T24 lines were purchased authenticated from ATCC. DLD-1 KRAS$^{WT/-}$, and DLD-1 KRAS$^{G13D/-}$ were purchased from Horizon Discovery, Ltd. MM415 and MM485 were authenticated by polymorphic short tandem repeat (STR) loci profiling by Promega. HEK-293T, CHL-1, SK-MEL-5, BxPC-3, AsPC-1, LS174T, HT-1376 and T24 are derived from female individuals. Caco-2, DLD-1, MM415, MM485, Capan-2 and SK-MEL-2 are derived from male individuals.

Primary human melanocytes were isolated from fresh biopsy samples approved by the Stanford University IRB and were propagated up to eight passages in Media 254 with HMGS supplement (Thermo Fisher Scientific Scientific) and 1% Pen-Strep. All primary

human melanocytes were male. All cell lines and primary cells were confirmed to be mycoplasma free bimonthly using the MycoAlert mycoplasma detection kit (Lonza).

METHOD DETAILS

Plasmids and Viral Transduction—All exogenous expression constructs were cloned into LentiORF pLEX-MCS-IRES-Puro (Open Biosystems Cat# OHS4735). The birA* sequence is as previously published (Roux et al., 2012) with the addition of a 10 amino acid Glycine/Serine linker before the Ras isoforms. The NRAS sequence was cloned out of pCGN N-Ras WT (Addgene #14723), HRAS and KRAS were cloned from existing lab stocks of pLEX vectors. To match expression of birA* H-Ras and N-Ras fusions with endogenous protein levels, a short upstream ORF (uORF) was added 5' to the coding region. BirA* fusion proteins were cloned into pLEX with an in frame HA-birA* tag to generate: pLEX-uORF-HA-birA*-H-Ras(wildtype), pLEX-uORF-HA-birA*-H-Ras(G12V), pLEX-HA-birA*-K-Ras(wildtype), pLEX-HA-birA*-K-Ras(G12D), pLEX-uORF-HA-birA*-N-Ras(wildtype), pLEX-uORF-HA-birA*-N-Ras(Q61K) and pLEX-uORF-HA-birA*-STOP controls Oncogenic and effector domain mutants were generated using inverse PCR mutagenesis followed by In-Fusion (Takara) of the mutation containing region at the 5' and 3' ends to generate T35A, E37A and Y40A in addition to the already present Q61K mutation.

The pLEX-FHH:NRAS point mutants used for pathway activity studies in primary melanocytes were also generated using inverse PCR mutagenesis on the wild-type plasmid followed by In-Fusion cloning of the PCR product (Takara). pLEX flag only NRAS plasmids were generated from the pLEX-FHH:NRAS template introducing a single FLAG-tag in the forward primer. pLEX FLAG-RHEB was cloned off a gBlock (IDT) template with an N-terminal FLAG-tag introduced via PCR.

For recombinant protein production, the target domains of interest were cloned out of their respective full length sequences pMSCV mSin1.1 HA (Addgene Cat# 12582), pcDNA3-Flag mTOR wt (Addgene Cat# 26603) and MGC Human RAF1 Sequence-Verified cDNA Clone ID: 3904404 (Dharmacon Cat# MHS6278-202756888). The domains- $RAF1^{RBD}$ (AA1-149), $MAPKAP1^{RBD}$(AA279-353), $MAPKAP1^{RBD}$/Triple Mutant (AA279-353; K307A,K310A,R312L), $MTOR^{HEAT}$(AA1-409), $MTOR^{KinaseDomain}$(AA1967-2549) - were cloned into pLEX-FHH-IRES-Puro with the tag on N-terminus using In Fusion Cloning.

ShRNA knockdown was done with either pGIPZ (Dharmacon) or pLKO.1 (Addgene) backbones as indicated. For pLKO.1 shRNA hairpin cloning, sense and anti-sense insert oligos were annealed and ligated into the cut backbone using T4 DNA ligase at room temperature for at least 1 hour.

For both exogenous expression and shRNA lentiviral production, 293T were transfected with 9 μg lentiviral expression construct, 7 μg pCMVΔ8.91, and 2.5 μg pUC MDG. Transfections were done in 10cm plates using Lipofectamine 2000 (Life Technologies). Viral supernatant was collected at 48 and 72 hours after transfection and concentrated using Lenti-X Concentrator (Takara). All cell lines were seeded into lentiviral-containing media and transduced overnight with 5 μg/mL polybrene with fresh media change the next

morning. Cells were selected using 1-5 μg/mL puromycin or blasticidin approximately 36 hours after initial infection.

Immunoblotting—For protein extraction, cells were lysed in 1× Cell Lysis Buffer (Cell Signaling, Cat# 9803) with Complete Mini Protease Inhibitor Cocktail, EDTA-free (Millipore Sigma) and PhosStop phosphatase inhibitor cocktail (Millipore Sigma). Cells were allowed to lyse on ice for at least 15 minutes followed by centrifugation at 16,000×g for 12 minutes. The soluble fraction was removed and quantified using the Pierce BCA Protein Assay Kit. 15-30ug of protein was loaded into a NuPAGE novex Bis-Tris gel (Thermo Fisher Scientific Scientific) and transferred to 0.45μM pore size Immobilon-FL PVDF membrane (Millipore Sigma). Membranes were blocked with Odyssey blocking buffer (PBS) (LI-COR) for at least 30 minutes at room temperature. Primaries were added to 5% BSA in TBST and incubated with the membrane overnight at 4C. The membranes were washed three times in TBST and incubated with LI-COR secondary antibodies- 800CW Goat anti-Mouse IgG (H + L), 800CW Goat anti-Rabbit IgG (H + L), 680RD Goat anti-Mouse IgG (H + L)- (1:15,000) in 5% milk in TBST for 45 minutes at room temperature. The membranes were washed twice in TBST and once in PBS then scanned on the Odyssey CLx. All quantification was done in the Image Studio Lite software.

The following antibodies were used: anti-P13 Kinase p110α (4249, Cell Signaling Technologies), anti-Raf-1 (C12) (sc-133, Santa Cruz Biotechnology), anti-HA (ab130275, Abcam), anti-HA (C29F4) (3724, Cell Signaling) anti-HRAS (C-20) (sc-520, Santa Cruz Biotechnology), anti-NRAS (C-20) (sc-519, Santa Cruz Biotechnology), anti-Pan-Ras (C-4) (sc-166691, Santa Cruz Biotechnology), anti-β-Actin (A1978, Millipore Sigma), anti-MTOR (2972, Cell Signaling Technology), anti-Rictor (A300-459A, Bethyl Laboratories), anti-MAPKAP1 (15463-1-AP, ProteinTech), anti-Raptor (A300-553A, Bethyl Laboratories), anti-Phospho-AKT (Ser473) (4060, Cell Signaling Technologies), anti-Phospho-AKT (Thr308) (13038, Cell Signaling Technologies), anti-Akt(pan) (2920, Cell Signaling Technologies), anti-Phospho-4E-BP1 (Thr37/46) (2855, Cell Signaling Technologies), anti-4E-BP1 (9644, Cell Signaling Technologies), anti-Phospho-NDRG1 (Thr346) (5482, Cell Signaling Technologies), anti-NDRG1 (9485, Cell Signaling Technologies), anti-NDRG1 (26902-1-AP, ProteinTech), anti-Phospho-p70 S6 Kinase (Thr389) (9205, Cell Signaling Technologies), anti-p70 S6 Kinase (2708, Cell Signaling Technologies), anti-Living Colors mCherry (632543, Takara), anti-Phospho-MEK1/2 (Ser217/221) (41G9) (9154, Cell Signaling), anti-MEK1/2 (9122, Cell Signaling), anti-Phospho-p44/42 MAPK (Erk1/2) (Thr202/Tyr204) (197G2) (4377, Cell Signaling), anti-p44/42 MAPK (Erk1/2) (3A7) (9107, Cell Signaling Technologies), anti-GST (26H1) (2624, Cell Signaling), and anti-FLAG M2 (F1804, Millipore Sigma).

Membrane-Cytoplasmic Cellular Fractionation—Fresh cell pellets were resuspended in digitonin lysis buffer (50 mM HEPES pH 7.5, 100 mg/mL digitonin, 150 mM NaCl) and rotated end-over-end at 4 °0 for 30 minutes. The lysed material was centrifuged at 6000×*g* for 5 minutes. The supernatant, containing the cytoplasmic material, was removed to a new tube. To remove nuclear material, the pellet was resuspended in 0.3% NP-40, 50mM HEPES pH 7.5 and 150 mM NaCl and left on ice for 5 minutes. The material was pelleted via

centrifugation at 1500×*g* for 2 minutes. The supernatant was removed as the membrane fraction.

Cell Titer Blue Growth Assay—Cell lines were seeded into 24-well plates at low density. The following morning (day 0) and every following day after seeding the media was changed to media containing cell titer blue reagent (Promega) per the manufacturer's protocol and allowed to incubate at standard tissue culture conditions for two hours. For each well, 100uL media was removed in triplicate into a 96-well plate and read at 560/590 on a spectrophotometer.

Proximity-Dependent Protein Labeling Methods

Mass Spectrometry Sample Preparation: CHL-1, HT-1376 and Caco-2 cells expressing constitutive, birA control or birA:Ras fusion proteins were treated with 50 μM biotin diluted in DMEM 10% FBS (CHL-1) or EMEM 10% FBS (HT-1376 & Caco-2) for 24 hours when the cells were at ~70-80% confluence. After 24 hours, the cells were harvested via two PBS washes, trypsinization, quenching, PBS wash and snap freezing. Preparation of lysates for streptavidin pulldown was carried out as previously described (Roux et al., 2013) with the addition of a 3K MWCO column filtration step just prior to addition to MyOne C1 streptavidin beads (Thermo Fisher Scientific) to remove excess free biotin. For mass spectrometry, 20-30mgs of total input protein were used with 1mL of MyOne C1 streptavidin beads and allowed to bind overnight (~16hrs). After binding, the samples were washed as described (Roux et al., 2013) and eluted in biotin elution buffer (1× NuPAGE LDS Sample Buffer, 20 mM DTT, 4 mM biotin). A portion of the sample was run on SDS-PAGE gel, transferred to PVDF membrane, and probed with 800CW streptavidin dye (LI-COR) to confirm induction of biotinylation.

For mass spectrometry, the samples were run on a 4-12% Bis-Tris SDS-PAGE gel and stained with Colloidal Blue Staining Kit (Thermo Fisher Scientific). Each sample was divided into 9 sections, minced and placed in 1% acetic acid. Each sample was in gel digested as previously described (Shevchenko et al., 2006), in brief samples were washed with 50mM ammonium bicarbonate, followed by reduction with DTT (5 mM) and alkylation using propionamide (10 mM). Gels were further washed with an acetonitrile/ ammonium bicarbonate buffer until all stain was removed. 125 ng of trypsin/LysC (Promega) reconstituted in 0.1% protease max (Promega) 50 mM ammonium bicarbonate was added to each gel band for overnight digestion. Peptides were extracted from the gels followed by SpeedVac until fully dry.

Mass Spectrometry: Peptide pools were reconstituted and injected onto a C18 reversed phase analytical column, ~25 cm in length packed in house using Reprosil Pur (Dr. Maisch). The UPLC was a Waters NanoAcquity, operated at 450nL/min using a linear gradient from 4% mobile phase B to 35% B. Mobile phase A consisted of 0.1% formic acid, water, Mobile phase B was 0.1% formic acid, water. The mass spectrometer was an Orbitrap Elite set to acquire data in a data dependent fashion selecting and fragmenting the 15 most intense precursor ions in the ion-trap where the exclusion window was set at 45 seconds and multiple charge states of the same ion were allowed.

LC-MS data analysis: MS/MS data were analyzed using both Preview and Byonic v2.6.49 (ProteinMetrics). All data were first analyzed in Preview to provide recalibration criteria if necessary and then reformatted to .MGF before full analysis with Byonic. Analyses used Uniprot canonical and isoform FASTA files for Human with mutant sequences concatenated as well as common contaminant proteins. Data were searched at 12 ppm mass tolerances for precursors, with 0.4 Da fragment mass tolerances assuming up to two missed cleavages and allowing for fully specific and N-ragged tryptic digestion. These data were validated at a 1% false discovery rate using typical reverse-decoy techniques (Elias and Gygi, 2007). The resulting identified peptide spectral matches and assigned proteins were then exported for further analysis using custom tools developed in MatLab (MathWorks) to provide visualization and statistical characterization.

Spectral match assignment files were collapsed to the gene level and false positive matches and contaminants were removed. SAINT analysis (Choi et al., 2011) (crapome.org) was run with the following parameters: 10,000 iterations, LowMode ON, Normalize ON and the union of MinFold ON and OFF. All available CRAPome birA controls (Nov 2015) were used in addition to the controls generated in this study as negative controls. Minimum interactome inclusion criteria were SAINT≥ 0.8, fold change over matched cell type control ≥ 4. Low normalized spectral count proteins were removed. Core common interactome protein candidates met these criteria in at least one Ras sample in all three isoform sets.

To define isoform versus cell type specificity, publicly available RNA-sequencing data was used for HT-1376 from the Cancer Cell Line Encyclopedia (CCLE) project and for Caco-2 from GEO (GSE48603). CHL-1 expression data was from this study. The data were normalized as a fraction of the whole to enable cross cell line data comparison. Using the expression levels of proximal Ras interactors identified in all three lines/isoforms, an upper threshold for relative cell line specific expression was set at the top 10%. This threshold was used to call likely isoform specific interactors- the gene is expressed in a cell line, but was not found in the proximal interactome. As opposed to likely cell type specific interactors- the protein was not identified in a given isoform interactome and the gene is not sufficiently expressed that cell line.

Protein Interactome Construction: All protein network interactomes were built in Cytoscape (v3.1.1). Known protein-protein interactions among Ras candidate proximal interactors were imported using the GeneMANIA App from the following sources, BioGRID Small Scale, BioGRID (iRef), BIND (iRef), and Pathway Commons. Redundant edges were removed. Protein-protein interactome enrichment statistical analysis was done using the STRING database online interface with experimental and database sources set to the high confidence threshold (0.7) (Szklarczyk et al., 2015). All GO Term analysis was done via Enrichr online portal (Chen et al., 2013b).

Crosslinking Mass Spectrometry

Sample preparation and Mass Spec Data Acquistion: N-Ras^{Q61K} (Origene) was diluted in PBS with 5mM GTPγS (Abcam) and incubated for 15 minutes at 30 °C. N-Ras ^{Q61K} was then combined at equimolar ratios with either mTOR or MAPKAP1 (Origene or homemade)

in PBS with BS3 at 0.2 or 0.5mM (Thermo Fisher Scientific). The mixture was incubated for 1 hour at 25 °C at 35 0 r.p.m. in a thermomixer. The reaction was quenched with the addition of 4× LDS, 10% beta-mercaptoethanol and heating at 75 °C for 15 minutes. The protein gels were stained with colloidal blue and the region containing the crosslinked complex was cut out. The preparation of the gel slice for mass spectrometry anlaysis was carried out as described above.

For the mass spectrometry, either a timsTOFpro (Bruker Corporation, Billerica, MA) with a nanoElute UPLC (Bruker Corporation, Billierica, MA) or a Orbitrap Fusion (Thermo Scientific, San Jose, CA) with a NanoAcquity M-Class UPLC (Waters Corporation, Milford, MA) was used to obtain tandem mass spectra of peptides present in each sample. A C18 reverse-phase column was used for both instruments, with mobile phases of 0.2% formic acid aqueous for Phase A and 0.2% formic acid in acetonitrile for Phase B. The timsTOFpro was operated in PASEF (parallel accumulation sequential fragmentation) mode, with mass tolerances of 50 ppm for both precursor and fragment ions. The Orbitrap fusion was operated with either collision-induced dissociation (CID) or electron transfer dissociation / higher-energy collisional dislocation (ETD/HCD) in a decision tree format for fragmentation to identify precursor peptides. Precursor and HCD were detected in the Orbitrap with 12 ppm mass tolerances, while CID and ETD were detected in the ion trap with 0.4 Da mass tolerances.

Crosslinked Peptide Data Analysis: In a typical analysis, raw mass spectral data were analyzed using Byonic (Protein Metrics, San Carlos, CA, v2.14.27) to assign peptides and infer proteins. Peptide data were restricted based on tryptic digestion, allowing for n-terminal ragged cleavages, and up to two missed cleavage sites. Proteins were held to a 1% false discovery rate. Byonic X-Link functionality was used to generate predicted crosslinks between biding partners. Data were further analyzed using Byologic (Protein Metrics, San Carlos, CA) for validation, visualization, and report generation. Potential crosslinks were graded empirically based on their log probabilities, their XIC, MS1, and MS/MS spectra, as well as other qualitative features such as the presence of potential collating peptides. The crosslinked peptides were assigned a confidence ranking. High confidence crosslinks were identified as true positives or identified more than twice with some uncertainty in the peptide call (short peptide or co-isolation) and in both cases were structurally consistent with interaction through the Switch I, Switch II, or effector binding region of Ras. Crosslinks detected twice with uncertain features and true positives with inconsistent 3D structural geometry were considered low confidence crosslinks.

CRISPR Proliferation Screen

Input Library construction: A custom sgRNA library was designed with 6 sgRNAs targeting each gene and 400 non-targeting controls. All sgRNA sequences were obtained from the Get-go v2 library (Sanjana et al., 2014). DNA oligo synthesis and pooled library cloning was performed similarly to previously described methods (Sanjana et al., 2014) using a lentiviral vector with increased sgRNA expression pSLQ1651-sgTelomere(F+E) (Chen et al., 2013a) with the mouse U6 promoter replaced with human U6 and the guide swapped for a stuffer (pLentiGuide; Addgene #117986). Cloning was performed at 10×

coverage and library complexity was verified by high-throughput sequencing. Nearly all (~99%) sgRNAs were present in the final plasmid library.

CRISPR Library Screen: Prior to infection with the CRISPR library, CHL-1, MM415, MM485, BxPC-3, AsPC1, Caco-2, LS174T, HT-1376, T24, and primary melanocytes we infected with pLEX_Cas9 (pLEX Cas9-FLAG-P2A-blasticidin; Addgene #117987) lentivirus at the highest tolerated dose, as determined by impact on growth compared to uninfected control cells. Subsequently, these cell lines and primary cells were infected with the lentiviral CRISPR library to achieve a MOI of ~0.3-0.4. Prior to infection for the full-scale screen, appropriate MOI was determined by viral titration and post-puromycin selection survival compared to unselected control cells. Library infected Cas9-expressing cells were selected in a cell line specific concentration of puromycin until all uninfected controls cells were dead (~48-72 hours). Cells sufficient for ~1000× library coverage per infection were taken as day 0 time point and two sets of cells for ~1000× library coverage were seeded for biological replicates to be carried through the CRISPR proliferation screen. Cells were split as needed dependent upon doubling time of cell line, replating a minimum of ~1000× library coverage/replicate. After 14 days, cells for ~1000× library coverage/ replicate were harvested, representing the end point of the proliferation screen. For each cell line, two independent infections were done with two day 14 samples taken per infection for a total of 4 replicate day 14 samples per line.

Sequencing library construction & sequencing: Genomic DNA was isolated using the DNeasy Blood and Tissue Isolation Kit (QIAGEN). For melanocyte samples, the gDNA was cleaned of melanin using the OneStep™ PCR Inhibitor Removal Kit (Zymo). To isolate the CRISPR guide cassette from the genome, PCR was done at one reaction for every 5×10^5 cells using PrimeSTAR Max DNA Polymerase Premix (Takara). At this time, a unique 9-mer barcode was added to each guide cassette amplicon for removal of PCR duplicates (Table S7). Subsequent to 5 cycles of PCR, the reactions were pooled over NucleoSpin Gel and PCR Clean-Up Columns (Takara). A second PCR of 23-25 cycles was done to prepare the DNA for flow cell binding, including barcoding for multiplexing, and sufficient amplification. Standard Illumina i5/i7 barcodes were used. This round of PCR was followed by PCR cleanup over a single column and run on a 2.5% agarose gel to isolate the single product band for high-throughput sequencing. When necessitated by Bioanalyzer trace results, a secondary PAGE purification was carried out via standard protocol and purified over PCR cleanup columns. Samples were sequenced to a minimum average per unique guide coverage of 100× on the NextSeq Platform.

CRISPR Data Analysis: CRISPR sequencing was analyzed by removing duplicates, trimming the reads, and aligning them to an indexed Bowtie (Langmead et al., 2009) library of the guide sequences. Read counts were compiled for each sgRNA in each sample. For each cell line, MAGeCK (Li et al., 2014) was run as a group of the individual replicates, resulting in 2 controls and 4 experimental conditions per cell line. MAGeCK was run in test mode with the –control-sgrna option. Gene summary files were used in downstream analysis. Negative selection FDR cutoff ≤ 0.18 is in line with previous publications (Li et al., 2014). Genes significant in both positive and negative selection screens were excluded.

Candidate proteins were ranked for follow up by a combined CRISPR and mass spectrometry score defined as *[1/ Oncogenic Cell Line Avg Negative Selection FDR]* [Avg log_2(Ras^{MT}PSM/Ras^{WT}PSM)]*.

Immunofluorescence and Proximity Ligation Assay—Cells were fixed with 4% Paraformaldehyde at room temperature for 10 minutes. Blocking was done in 5% goat serum, 0.3% TritonX-100 in PBS for one hour. For Raf1, mTOR and mTOR complex PLA experiments, cells were placed in 0% FBS media overnight (~16hrs) and stimulated for 15 minutes with 10% FBS media prior to fixation. Formalin-fixed, paraffin embedded colorectal adenocarcinoma patient tissue samples were rehydrated in xylene and decreasing dilutions of ethanol followed by Citrate Buffer (pH 6.0) antigen retrieval (Abeam). Specimens were blocked in 5% goat serum, 0.3% Triton X-100 in PBS for one hour. For both cell and tissue PLA, anti-mouse PLUS and anti-rabbit MINUS Duolink secondaries with Duolink *In Situ* Orange Reagents were used according to the manufacturers protocol (Millipore Sigma). For Ki67 staining, cells were seeded onto glass slides and on day 3 of puromycin selection were starved for 22 hours. Cells fixed with 4% PFA for 15 minutes and were blocked in 5% goat serum, 5% horse serum, 0.3% Triton X-100 in PBS for 1 hour. Primary antibodies were as follows: anti-Ki67 (1:250; Thermo Fisher Scientific, RM-9106), anti-Pan-Ras (C-4) (1:50; sc-166691, Santa Cruz Biotechnology), anti-Raf-1 (C12) (1:200; sc-133, Santa Cruz Biotechnology), anti-WASL (1:500; 14306-1-AP, ProteinTech), anti-MARK2 (1:200; HPA038790, Millipore Sigma), anti-NUMB (1:1000; ab14140, Abcam), anti-EHBP1 (1:500; 17637-1-AP, ProteinTech), anti-RAFT1 (1:100; 611132, BD Transduction Laboratories), anti-MTOR (1:2000; ab2732, Abcam), anti-Rictor (1:5000; A300-459A, Bethyl Laboratories), anti-SIN1 (1:1000; A300-910A, Bethyl Laboratories) and anti-Raptor (1:1000; 20984-1-AP, ProteinTech). Anti-Active Ras (1:1000; 26909, NewEast Biosciences) has been reported as thoroughly validated to specifically recognizes Ras-GTP and not Ras-GDP in immunofluorescence experiments. Ki67 positive cells and PLA particle count and percent area signal were quantified using Fiji ImageJ (Schindelin et al., 2012) and normalized to the number of nuclei per field or percent DAPI area per field as indicated in the figure. For immunofluorescence (IF), PLA experiment matched slides were treated as above and incubated with anti-Mouse Alexa Fluor 555 and anti-Rabbit Alexa Fluor 488 (1:5000; Thermo Fisher Scientific) for 1 hr at room temperature.

Far Western Blots—Prior to membrane deposition, recombinant KRAS^{G12D} (Origene), NRAS^{Q61K} (Origene), HRAS^{G12V} (Origene) and GST (Millipore Sigma) were diluted in PBS with 5mM GTPγS (Cytoskeleton, Inc.) and incubated for 15 minutes at 30 °C. The indicated amount of KRAS ^{WT} (Abcam), NRAS^{WT} (Origene), HRAS^{WT} (Origene), MT Ras or control GST were spotted onto nitrocellulose membrane and allowed to air dry. Duplicate spotted membranes were either stained with colloidal gold per manufacturer's instructions (Bio-Rad) or blocked for two hours at room temperature in 5% milk in TBST. Subsequently, the blocked membrane was incubated overnight at 4 °C with 1 μg of recombinant mTOR protein (Origene) per 1mL of 5% milk in TBST. After protein incubation, the membranes were washed in TBST and incubated with anti-MTOR (1:1000; 2972, Cell Signaling Technology) primary antibody at 4 °C overnight. The membrane was washed the next day, incubated with horseradish peroxidase (HRP)-conjugated secondary antibody for 1 hour at

room temperature and then washed. Signal was developed using SuperSignal West Dura reagent (Thermo Fisher Scientific). After development, the membrane was probed with anti-Pan-Ras (C-4) antibody (1:1000) overnight and developed using LI-COR 800 anti-mouse secondary to quantify total Ras protein loading. All far western signal quantification was done using ImageStudio Lite software (LI-COR) and normalized to total Ras protein loading.

For Ras effector Far Western experiments, the indicated amount of MAPKAP1 (Origene), mTOR (Origene), PI3Kγ (Origene), RalGDS (Origene), RAF1 (Origene), GST (Millipore Sigma), mLST8 (Abnova) or Akt (Jena Bioscience) were spotted onto nitrocellulose membrane and allowed to air dry. Duplicate spotted membranes were either stained with colloidal gold per manufacturer's instructions (Bio-Rad) or blocked for two hours at room temperature in Odyssey Blocking Buffer (PBS) (LI-COR). Subsequently, the blocked membrane was incubated overnight at 4 °C with 1 μg of GTPγS-loaded $NRAS^{Q61K}$ (Origene) per 1mL of Odyssey Blocking Buffer (PBS) with 0.1%Tween. After protein incubation, the membranes were washed in TBST and incubated at 1hr at room temperature with anti-Pan-Ras (C-4) antibody followed by development with LI-COR 800 anti-mouse secondary.

Microscale Thermophoresis Experiments—All recombinant target proteins were produced in 293T cells. Briefly, 20μg of pLEX FHH-tagged target protein plasmid was transfected per 15cm plate of ~80% confluent 293T cells, using polyethyleneimine (PEI). After 48 hours, the cells were lysed on plate (50mM Tris pH 7.4, 150mM NaCl, 5mM EDTA, 1% Triton X-100, 10% Glycerol, 1mM DTT, Complete Protease Inhibitor Cocktail, EDTA-free), scraped into eppendorf tubes and lysed rotating at 4C for 30 minutes. The lysate was centrifuged at 16,000×g for 10 minutes and quantified. The lysate was added to a saturating volume of anti-FLAG M2 affinity gel (Millipore Sigma), which was determined by a small scale, pilot IP for each protein. The IP went overnight at 4C and the next morning was washed three times with wash buffer (50mM Sodium Phosphate pH 7.4, 5mM EDTA, 1% Triton X-100, 300mM NaCl, 10% Glycerol, 1mM DTT). The M2 beads were primed with one wash of Elution Buffer (50mM Sodium Phosphate pH 7.4, 100mM NaCl, .01% Tween-20). The protein was eluted with 0.5mg/mL 3XFLAG peptide in Elution Buffer once at 4 times the bead volume for 1 hour followed by a second elution at 2 times bead volume for 15 minutes. The two rounds of eluates were pooled and concentrated using 10k molecular weight cutoff Amicon columns (Millipore). The target protein concentration was determined against a BSA standard curve run on a Bis-Tris gel and stained using InstantBlue Protein Stain (Expedeon).

For microscale thermophoresis (MST) experiments, the protein was labeled using the Monolith His-Tag Labeling Kit RED-tris-NTA (Nanotemper Technologies) following the manufacturer's protocol at a 1:2 dye to protein ratio. The concentrated was based on the BSA standard curve quantification with a final concentration of 100nM labeled protein. The level of label signal was checked via a capillary scan at 60% LED power and diluted to 600 units using the provided 1× PBST, resulting in a target protein concentration ~40nM. The H-Ras^{WT} protein (Cytoskeleton, Inc.) was loaded with either 1.5mM GDP (Abcam) or GTPγS (Abcam) in 2mM Tris pH 7.6 and 20mM EDTA at 30C for 1 hour at 300 rpm. Subsequently,

the loading was quenched on ice for 2 minutes and supplemented with $MgCl_2$ to 65mM final. The H-Ras protein was buffer exchanged into (25mM pH 7.4 Sodium Phosphate, 50mM NaCl, 1mM DTT, 5mM $MgCl_2$, 0.05% Tween) via 10k molecular weight cutoff columns with 3 full exchanges. The loaded protein was quantified on an InstantBlue stained protein gel against a standard curve of the pre-loaded H-Ras stock protein. A series of 16 1:1 dilutions of the H-Ras protein (the ligand) was prepared using the exchange buffer. For the measurement, each ligand dilution was mixed with one volume of labeled protein, which lead to a final concentration of ~20 nm. The mixed samples were incubated for ~5 minutes at room temp and were loaded into Monolith NT.115 Premium Capillaries (NanoTemper Technologies). MST was measured using a Monolith NT.115 instrument (NanoTemper Technologies) at an ambient temperature of 25°C Instrument parameters were adjusted to 50 or 60 % LED power and 40 % MST power. Data of at least three independently pipetted measurements were analyzed (MO.Affinity Analysis software, NanoTemper Technologies) using the signal from an MST-on time as indicated in the legend.

Expression Profiling & RNA-Seq Data Analysis—For RNA sequencing, cells were selected for 72 hours with 1μg/mL puromycin and harvested approximately 108 hours after infection with shRNA hairpin or exogenous expression construct. RNA was isolated using the RNeasy Plus Kit (QIAGEN). RNA sequencing libraries were prepared with TruSeqv2 library preparation kit (Illumina) and sequenced with the Illumina HiSeq4000 platform using 150-bp paired-end sequencing. Alignment was performed with TopHat2 (Kim et al., 2013), and Cuffdiff2 (Trapnell et al., 2013) was used to call differential gene expression. All genes included in heatmaps and signatures changed by at least 2 fold in one sample with the other matched replicate sample changing concordantly.

GSEA Methods—GSEA was run with 1000 permutations, using gene set permutation and weighted Signal2Noise metrics. When gene sets were large and user defined gene signatures were used as the gene set database, the maximum gene set size was increased to 1000. Inputs from RNA Sequencing always included the full FPKM table, and inputs from the TCGA included the publicly available gene matrix, sorted to match the defined phenotypes.

Co-Immunoprecipitation (Co-IP)—CHL-1 cells were infected with a titration series of pLEX uORF-FHH-empty vector, N-terminal pLEX-uORF-FLAG-HA-HIS (FHH) $NRAS^{WT}$ fusion, or pLEX-uORF-FHH:$NRAS^{Q61K}$ fusion lentivirus. MM415 and MM485 cells were infected with a titration series of pLEX uORF-FHH-empty vector or pLEX uORF-FHH-$NRAS^{Q61K}$ fusion lentivirus. All cells were selected with 1 μg/mL puromycin and kept as a stably expressing bulk population under selection. FHH:N-Ras construct expression was assayed in the bulk population and the titration expressing most closely to endogenous N-Ras protein levels was selected along with the matched empty vector titration. When at 70-80% confluence, the cells were fixed on plate in 0.5% formaldehyde for 15 minutes at room temperature while rocking. The crosslinking was quenched with 125mM glycine final for 5 minutes. The plates were washed twice with ice cold PBS and the cells were lysed on plate with CHAPS IP lysis buffer (25mM Tris pH 7.4, 150mM NaCl, 1% NP-40, 1mM EDTA and 5% glycerol). Cells were scraped into eppendorf tubes and allowed to lyse, rotating at 4C for at least 15 mins. After centrifugation to remove insoluble material and

quantification, 1.5mg of lysate was added to 50uL of anti-HA Agarose Bead slurry (Thermo Fisher Scientific). After overnight IP, the beads were washed 3 times with lysis buffer and eluted with elution buffer pH 2.8 (Thermo Fisher Scientific).

The MM485 cell line was infected with pLEX empty vector, MAPKAP1 Isoform 1 full length or a deletion that maintains amino acids 1-192. All constructs contained a c-terminal FLAG-HA-HIS (FHH) fusion. After 3 days of puromycin selection, cells were starved overnight in 0% FBS media. The next morning the cells were stimulated with 10% FBS media for 10 minutes, lysed in CHAPS Lysis Buffer (50 mM Tris pH7.5, 150 mM NaCl, 0.3% CHAPS, 10 mM $MgCl_2$) and centrifuged to remove the insoluble fraction. Lysate was added to anti-HA Agarose Beads (Thermo Fisher Scientific) and incubated for 4 hours at 4C. The beads were washed 3 times in lysis buffer and eluted in LDS sample buffer at 75 °C for 15 minutes.

***In Vitro* mTORC2 IP-Kinase Assays—**To generate mTORC2 complexes for *in vitro* IP-kinase assays, 293T cells were seeded into 15cm plates and PEI transfected with 20μg pLEX FHH-EV or pLEX-MAPKAP1^{WT}-FHH vector along with 5μg pLEX FHH-EV, pLEX-FLAG-NRAS^{WT}, pLEX-FLAG-NRAS^{Q61K} or pLEX-FLAG-RHEB^{WT} for the co-expression IP-kinase experiments. ~48 hours after transfection the cells were lysed on plate in CHAPS IP-kinase lysis buffer (25mM HEPES pH 7.5, 150 mM NaCl, 1mM EDTA, 0.3% CHAPS). Cells were scraped into eppendorf tubes and allowed to lyse, rotating at 4C for at least 15 minutes. The lysate was centrifuged at 16,000×g for 12 minutes and the soluble fraction removed and quantified. For each kinase reaction, 0.75mg of lysate was added to 12uL of Pierce anti-HA magnetic beads (Thermo Fisher Scientific). The IP proceeded for approximately 4 hours for the co-expression experiments or overnight for the recombinant Ras addition experiments. After IP, the beads were washed 3 times with lysis buffer followed by one kinase buffer wash (50mM HEPES pH 7.5, 10mM $MgCl_2$).

For the co-expression mTORC2 IP-kinase assay, all reactions were pre-treated with 10uL of either DMSO or 5μM PP242 (Selleck Chemicals) diluted in kinase reaction buffer (50mM HEPES pH7.5, 2mM DTT, 10mM $MnCl_2$, 10mM $MgCl_2$) at 30C with 15 seconds at 1250rpm and 2 minutes rest. After 15 minutes incubation, 10uL of kinase reaction with 2ug of GST-Akt1-tail-AA409-480 was added to achieve a final concentration of 200μM ATP and 5μM PP242 or equivalent DMSO. The kinase reaction was allowed to proceed for 45 minutes followed by quenching with 4× LDS loading buffer. Phosphorylation was analyzed via immunoblotting as described above.

For recombinant H-Ras kinase experiments, the wild-type His-H-Ras (Enzo Life Sciences) protein was loaded with 5mM GDP (Abcam) and GST-H-Ras^{G12V} (Abcam) with 5mM GTPγS (Abcam) both in 50mM Tris pH 7.4, 45mM NaCl and 20mM EDTA at 30C for 1 hour at 300 rpm. After loading, the reaction was quenched with 70mM final $MgCl_2$ on ice. The H-Ras proteins were buffer exchanged as described above for MST experiments into 50mM HEPES pH 7.5, 2mM DTT, 10mM $MnCl_2$ and 10mM $MgCl_2$. 500ng of H-RasWT or H-Ras^{G12V} were added to each kinase reaction as indicated. Reactions without H-Ras protein were incubated with a GTPγS blank that was carried in parallel during nucleotide loading and buffer exchange. The mTORC2 complex IP was pre-incubated with buffer, wild-

type H-Ras or G12V H-Ras protein brought up to 10uL final with kinase reaction buffer. After 20 minutes of pre-incubation on ice, the kinase reaction mix with 1.5ug of GST-Akt1-tail per reaction and 200μM ATP final was added. The kinase reaction was allowed to proceed for 30 minutes followed by quenching with 4× LDS loading buffer.

LocaTOR2 mTORC2 In Cell Kinase Assay—MM485 LocaTOR2 cells were generated via pLEX-Frb:Akt2 infection and hygromycin selection (5 μg/mL) followed by infection with pLEX-FKBP localization constructs under blasticidin selection (1 μg/mL). The template Frb-Akt2 and FKBP-Localizer constructs were a gift of I. Yudushkin. The proteins or protein domains used to target each compartment were $KRAS^{C30}$ (plasma membrane), $Bcl\text{-}X_L{}^{C33}$ (mitochondria), Rab7 (late endosome), Rab5 (early endosome), Rab11 (recycling endosome) and TcR-β (endoplasmic reticulum). To induce heterodimerization and minimize off-target effects, cells were treated with 50nM AP21967 for 40 minutes, washed with cold PBS and lysed on plate. KU-0063794 (Selleck Chemicals) pre-treatment done for 1hr at 500 nM and continued throughout AP21967 treatment. All knockdown and MAPKAP1 expression experiments were done after three days of puromycin selection. All LocaTOR2 $pAkt^{S473}$ signal was normalized to LocaTOR2 total Akt signal and induction was quantified as fold over mock-treated matched sample.

Tumorigenesis Studies—CHL-1, MM485, SK-MEL-2, HT-1376, T24, DLD-1 $KRAS^{WT/-}$, and DLD-1 $KRAS^{G13D/-}$ cells were stably infected with a lentiviral vector containing firefly luciferase (pRRL Luciferase) and subsequently transduced with puromycin-selectable pLEX empty vector, pLEX-$MAPKAP1.1^{WT}$-FHH (Isoform 1) or pLEX-$MAPKAP1^{Del}$-FHH (FLAG-HA-HIS). Either 1×10^6 for MM485, CHL-1, and SK-MEL-2, or 3×10^6 for HT-1376, T24, and both DLD-1 lines were suspended in a 1:1 solution of PBS and Matrigel (BD Biosciences) and injected into the subcutaneous space of SHO mice (Charles River Laboratories). Tumor viability was measured using the *in vivo* imaging system IVIS-200 (Xenogen). Max average radiance from defined regions of interest was quantified using LivingImage 4.5 (Caliper LifeSciences). Once palpable, tumor volume was measure with electronic calipers and calculated using the formula $(L/2)\times(W/2)\times(H.2)\times(4/3)_{XTT}$. Animals were sacrificed before the mean diameter of the tumor reached 17.5 mm. Animal cohort numbers were chosen based on results from tumorigenesis pilot studies in mice. Researchers were not blinded to group identity.

Tumor Protein Lysate Preparation—Snap frozen subcutaneous tumor specimens were thawed in modified RIPA buffer (50 mM Tris pH8.0, 250 mM NaCl, 1% IGEPAL, 1 mM EDTA, 1% sodium deoxycholate, 0.1% SDS), minced, and transferred to Lysing Matrix D (MP Biomedicals) for FastPrep dissociation. Samples were cleared via centrifugation, sonicated, and again cleared by centrifugation. Immunoblotting was carried out as described above.

QUANTIFICATION AND STATISTICAL ANALYSIS

Graphed data are expressed as mean ± SEM unless indicated otherwise in the figure legends. The sample size (n) indicated in the figure legends represents biological replicates, experimental replicates or independent fields as appropriate and specified. Sample size was

determined by the preliminary experimental results and no statistical methods were used to predetermine sample size. All samples meeting basic experimental conditions and baseline quality control were included in the graphed data and statistical analysis. The statistical analyses described in each figure legend were performed using GraphPad Prism 7. With the exception of the MAGeCK CRISPR screen analysis, as described above, significance was accepted at the 95% confidence level (* $p < 0.05$, ** $p < 0.01$, *** $p < 0.001$, **** $p < 0.0001$). The statistical tests used are specified in the figure legend and are in agreement with the distribution of the data. The unpaired two-tailed t-test was used when comparing two groups unless the variances were unequal when a Welch's t-test was used. For the qPCR panel, the Holm-Sidak corrected p-value was calculated to control for multiple comparisons. For comparing multiple groups, a one-way ANOVA with Tukey's post-test was used. The Mann-Whitney U nonparametric test was used when the values in the two groups were not normally distributed. For the far western data, the Wilcoxon paired signed rank test was used as each value was paired within a given experimental replicate. Gene ontology p-values were determined using Fisher's Exact Test with Bonferroni correction using Enrichr (Chen et al., 2013b).

DATA AND SOFTWARE AVAILABILITY

RNA sequencing from this work has been deposited into the Sequence Read Archive with accession number SRP156923. Raw data have been deposited to Mendeley Data and are available at http://dx.doi.org/10.17632/kzxnrmh7fc.1.

KEY RESOURCES TABLE

REAGENT or RESOURCE	SOURCE	IDENTIFIER
Antibodies		
Ki67	ThermoFisher	Cat# RM-9106; RRID:AB_2341197
Pan-Ras (C-4) (PLA and western)	Santa Cruz Biotechnology	Cat# sc-166691; RRID:AB_2154229
Raf-1 (C12) (PLA and western)	Santa Cruz Biotechnology	Cat# sc-133; RRID:AB_632305
WASL	ProteinTech	Cat# 14306-1-AP; RRID:AB_10638478
MARK2	Sigma-Aldrich	Cat# HPA038790; RRID:AB_10674840
NUMB	Abcam	Cat# ab14140; RRID:AB_443023
EHBP1	ProteinTech	Cat# 17637-1-AP; RRID:AB_2097216
RAFT1	BD Transduction Laboratories	Cat# 611132; RRID:AB_398443
MTOR (PLA)	Abcam	Cat# ab2732; RRID:AB_303257
SIN1 (PLA)	Bethyl Laboratories	Cat# A300-910A; RRID:AB_661901
Raptor (PLA)	ProteinTech	Cat# 20984-1-AP; RRID:AB_11182390
MTOR (western)	Cell Signaling Technologies	Cat# 2972; RRID:AB_330978
P13 Kinase p110α	Cell Signaling Technologies	Cat# 4249; RRID:AB_2165248
HA-tag (C29F4) (Rabbit)	Cell Signaling Technologies	Cat# 3724; RRID:AB_1549585
HA-tag (Mouse)	Abcam	Cat# ab130275; RRID:AB_11156884
HRAS (C-20)	Santa Cruz Biotechnology	Cat# sc-520; RRID:AB_631670
NRAS (C-20)	Santa Cruz Biotechnology	Cat# sc-519; RRID:AB_632073
β-Actin	Sigma-Aldrich	Cat# A1978; RRID:AB_476692
Rictor (PLA and western)	Bethyl Laboratories	Cat# A300-459A; RRID:AB_2179967
MAPKAP1 (western)	ProteinTech	Cat# 15463-1-AP; RRID:AB_10598466
Raptor	Bethyl Laboratories	Cat# A300-553A; RRID:AB_2130793
Phospho-AKT (Ser473)	Cell Signaling Technologies	Cat# 4060; RRID:AB_2315049
Phospho-AKT (Thr308)	Cell Signaling Technologies	Cat# 13038; RRID:AB_2629447
Akt(pan)	Cell Signaling Technologies	Cat# 2920; RRID:AB_1147620
Phospho-4E-BP1 (Thr37/46)	Cell Signaling Technologies	Cat# 2855; RRID:AB_560835
4E-BP1	Cell Signaling Technologies	Cat# 9644; RRID:AB_2097841
Phospho-NDRG1 (Thr346)	Cell Signaling Technologies	Cat# 5482; RRID:AB_10693450
NDRG1	Cell Signaling Technologies	Cat# 9485; RRID:AB_2721143
NDRG1	ProteinTech	Cat# 26902-1-AP
Phospho-p70 S6 Kinase (Thr389)	Cell Signaling Technologies	Cat# 9205; RRID:AB_330944
p70 S6 Kinase	Cell Signaling Technologies	Cat# 2708; RRID:AB_390722
Living Colors mCherry	Takara	Cat# 632543; RRID:AB_2307319
Phospho-MEK1/2 (Ser217/221) (41G9)	Cell Signaling	Cat# 9154; RRID:AB_2138017
MEK1/2	Cell Signaling	Cat# 9122; RRID:AB_823567
Phospho-p44/42 MAPK (Erk1/2) (Thr202/Tyr204) (197G2)	Cell Signaling	Cat# 4377; RRID:AB_331775
p44/42 MAPK (Erk1/2) (3A7)	Cell Signaling	Cat# 9107; RRID:AB_2235073
GST (26H1)	Cell Signaling	Cat# 2624; RRID:AB_2189875

REAGENT or RESOURCE	SOURCE	IDENTIFIER
FLAG M2	Sigma-Aldrich	Cat# F1804; RRID:AB_262044
800CW Goat anti-Mouse IgG (H + L)	LI-COR	Cat# 926-32210; RRID:AB_621842
800CW Goat anti-Rabbit IgG (H + L)	LI-COR	Cat# 926-32211; RRID:AB_621843
680RD Goat anti-Mouse IgG (H + L)	LI-COR	Cat# 926-68070; RRID:AB_10956588
Duolink In Situ PLA Probe Anti-Mouse PLUS	Millipore Sigma	Cat# DUO92001
Duolink In Situ PLA Probe Anti-Rabbit MINUS	Millipore Sigma	Cat# DUO92005
Goat anti-mouse IgG (H+L)	Thermo Fisher Scientific	Cat# A21422; RRID:AB_2535844
Goat anti-Rabbit IgG (H+L)	Thermo Fisher Scientific	Cat# A11008; RRID:AB_143165
Bacterial and Virus Strains		
Biological Samples		
Colorectal adenocarcinoma tissue specimens	Asterand Biosceinces (BioIVT)	N/A
Discard Surgical Skin Tissue	Stanford University	N/A
Chemicals, Peptides, and Recombinant Proteins		
Medium 254	Thermo Fisher Scientific	Cat# M254500
Human Melanocyte Growth Supplement (HMGS)	Thermo Fisher Scientific	Cat# S0025
Lipofectamine 200	Thermo Fisher Scientific	Cat# 11668019
Lenti-X Concentrator	Takara	Cat# 631232
10× Cell Lysis Buffer	Cell Signaling Technologies	Cat# 9803
cOmplete, Mini, EDTA-free Protease Inhibitor Cocktail	Millipore Sigma	Cat# 11836170001
PhosStop	Millipore Sigma	Cat# 4906837001
800CW Streptavidin	LI-COR	Cat# 926-32230
Dynabeads MyOne Streptavidin C1	Thermo Fisher Scientific	Cat# 65002
Trypsin/Lys-C Mix	Promega	Cat# V5071
ProteaseMAX	Promega	Cat# V2071
$NRAS^{Q61K}$ Human Recombinant Protein	Origene	Cat# TP701004
NRAS Human Recombinant Protein	Origene	Cat# TP302681
MAPKAP1 Human Recombinant Protein	Origene	Cat# TP311745
mTOR Human Recombinant Protein	Origene	Cat# TP320457
$KRAS^{G12D}$ Human Recombinant Protein	Origene	Cat# TP700052
$HRAS^{WT}$ Human Recombinant Protein	Origene	Cat# TP316409
$HRAS^{G12V}$ Human Recombinant Protein	Origene	Custom Production from clone Cat# RC400129
GST protein, tag-free	Millipore Sigma	Cat# SRP5348
Human KRAS full length protein	Abcam	Cat# ab90768
PI3Kγ Human Recombinant Protein	Origene	Cat# TP307790

REAGENT or RESOURCE	SOURCE	IDENTIFIER
RalGDS Human Recombinant Protein	Origene	Cat# TP316933
RAF1 Human Recombinant Protein	Origene	Cat# TP301983
MLST8 (Human) Recombinant Protein	Abnova	Cat# H00064223-P01
Akt1	Jena Bioscience	Cat# PR-325
GTP-γ-S	Abcam	Cat# ab146662
GTP-γ-S	Cytoskeleton, Inc	Cat# BS01
BS3, No-Weigh Format	Thermo Fisher Scientific	Cat# 21585
PrimeSTAR Max DNA Polymerase	Takara	Cat# R045B
Antigen Retrieval Buffer (100× Citrate Buffer pH 6.0)	Abcam	Cat# ab93678
SuperSignal West Dura Reagent	Thermo Fisher Scientific	Cat# 34075
ANTI-FLAG M2 Affinity Gel	Millipore Sigma	Cat# A2220
Amicon Ultra-0.5 mL Centrifugal Filters	Millipore Sigma	Cat# UFC501096
Colloidal Gold Total Protein Stain	Bio-Rad	Cat# 1706527
InstantBlue Protein Stain	Expedeon	Cat# ISB1L
GDP	Abcam	Cat# ab146529
Pierce Anti-HA Agarose	Thermo Fisher Scientific	Cat# 26182
Pierce Anti-HA Magnetic Beads	Thermo Fisher Scientific	Cat# 88837
Torkinib (PP242)	Selleck Chemicals	Cat# S2218
GST-Akt1tail-AA409-480	GenScript	Custom Production
H-Ras (wild-type) (human), (recombinant) [IP-Kinase]	Enzo Life Sciences	Cat# BML-SE131-0100
Recombinant H-Ras (G12V) protein (GST Tagged) [IP-Kinase]	Abcam	Cat# ab90627
AP21967 (A/C Heterodimerizer)	Takara	Cat# 635055
KU-0063794	Selleck Chemicals	Cat# S1226
BD Matrigel Matrix	BD Biosciences	Cat# 354234
H-Ras protein: His tagged: human wild type (MST)	Cytoskeleton, Inc	Cat# RS01
Critical Commercial Assays		
MycoAlert Mycoplasma Detection kit	Lonza	Cat# LT07-318
In-Fusion HD Cloning Plus	Takara	Cat# 638909
Pierce BCA Protein Assay Kit	Thermo Fisher Scientific	Cat# 23225
Colloidal Blue Staining Kit	Thermo Fisher Scientific	Cat# LC6025
DNeasy Blood and Tissue Isolation Kit	QIAGEN	Cat# 69506
OneStep PCR Inhibitor Removal Kit	Zymo	Cat# D6030
NucleoSpin Gel and PCR Clean-Up	Takara	Cat# 740609.250
Duolink In Situ Detection Reagents Orange	Millipore Sigma	Cat# DUO92007
Monolith His-Tag Labeling Kit RED-tris-NTA	Nanotemper Technologies	Cat# MO-L008
TruSeq RNA Library Prep Kit v2	Illumina	Cat# RS-122-2001

REAGENT or RESOURCE	SOURCE	IDENTIFIER
CellTiter-Blue Cell Viability Assay	Promega	Cat# G8080
Deposited Data		
Cell Line RNA Sequencing Data	This paper	Sequence Read Archive: SRP156923
HT-1376 RNA Sequencing Data	Cancer Cell Line Encylopedia	https://portals.broadinstitute.org/ccle/data
Caco-2 RNA Sequencing Data	Gene Expression Omnibus (GEO) repository	GSE48603
Ras Proximity Proteomics Peptide Counts	This paper	Table S1
CRISPR Screen Unique Guide Counts	This paper	Table S2
Crosslinking Mass Spectrometry Data	This paper	Table S4
Primary Melanocyte Gene Level Expression Data	This paper	Table S5
Mutation and expression analysis of melanoma.	Cancer Genome Atlas Research Network	https://portal.gdc.cancer.gov/projects/TCGA-SKCM
Bladder carcinoma, colon adenocarcinoma & melanoma Ras allele mutations.	Catalogue of Somatic Mutations in Cancer (COSMIC) v.72	https://cancer.sanger.ac.uk/cosmic
Raw Images of Data	This study, Mendeley Data	http://dx.doi.org/10.17632/kzxnrmh7fc.1
Experimental Models: Cell Lines		
Human: CHL-1	ATCC	CRL-9446
Human: HEK-293T	Lab stock	N/A
Human: HT-1376	ATCC	CRL-1472
Human: Caco-2	ATCC	HTB-37
Human: SK-MEL-2	ATCC	HTB-68
Human: LS 174T	ATCC	CL-188
Human: BxPC-3	ATCC	CRL-1687
Human: MM415	CellBank Australia	CBA-1351
Human: MM485	CellBank Australia	CBA-1355
Human: AsPC-1	ATCC	CRL-1682
Human: DLD-1 $KRAS^{+/-}$	Horizon Discovery	HD 105-002
Human: DLD-1 $KRAS^{G13D/-}$	Horizon Discovery	HD 105-011
Human: T24	ATCC	HTB-4
Human: SK-MEL-5	ATCC	HTB-70
Human: Capan-2	ATCC	HTB-80
Primary Melanocytes	Stanford University	N/A
Experimental Models: Organisms/Strains		
Mouse: SCID Hairless Outbred (SHO) Crl:SHO-$Prkdc^{scid}Hr^{hr}$	Charles River Laboratories	474
Oligonucleotides		
shRNA sequences, see Table S7	This study	N/A
qPCR primers, see Table S7	This study	N/A
CRISPR Library Construction Primers, see Table S7	This study	N/A

REAGENT or RESOURCE	SOURCE	IDENTIFIER
Recombinant DNA		
pLKO.1 - TRC cloning vector (Puro). See Table S7 for shRNA sequences.	Addgene	Cat#10878
pLKO.1-blast	Addgene	Cat #26655
pLKO.1 shSCR	Addgene	Cat #17920
pLKO.1 GFP shRNA (Puro)	Addgene	Cat #30323
GIPZ Non-silencing Lentiviral shRNA Control	Dharmacon	Cat # RHS4346
GIPZ NRAS shRNA V3LHS_402088	Dharmacon	Cat # RHS4531-EG4893
GIPZ NRAS shRNA V2LHS_152358	Dharmacon	Cat # RHS4531-EG4893
GIPZ HRAS shRNA V3LHS_641012	Dharmacon	Cat# RHS4531-EG3265
GIPZ HRAS shRNA V3LHS_645806	Dharmacon	Cat# RHS4531-EG3265
LentiORF pLEX-MCS-IRES-Puro	Open Biosystems	Cat# OHS4735
pCGN N-Ras WT	Addgene	Cat# 14723
pLEX-uORF-HA-birA*-STOP-IRES-Puro	This Paper	Addgene Cat# 120558
pLEX-uORF-HA-birA*-H-Ras(wildtype)-IRES-Puro	This paper	Addgene Cat# 120559
pLEX-uORF-HA-birA*-H-Ras(G12V)-IRES-Puro	This paper	Addgene Cat# 120560
pLEX-HA-birA*-K-Ras(wildtype)-IRES-Puro	This paper	Addgene Cat# 120561
pLEX-HA-birA*-K-Ras(G12D)-IRES-Puro	This paper	Addgene Cat# 120562
pLEX-uORF-HA-birA*-N-Ras(wildtype)-IRES-Puro	This paper	Addgene Cat# 120563
pLEX-uORF-HA-birA*-N-Ras(Q61K)-IRES-Puro	This paper	Addgene Cat# 120564
pLEX-uORF-HA-birA*-N-Ras(Q61K/T35A)-IRES-Puro	This paper	Addgene Cat# 120565
pLEX-uORF-HA-birA*-N-Ras(Q61K/E37A)-IRES-Puro	This paper	Addgene Cat# 120566
pLEX-uORF-HA-birA*-N-Ras(Q61K/Y40A)-IRES-Puro	This paper	Addgene Cat# 120567
pLEX-FHH-Empty Vector-IRES-Puro	This paper	Addgene Cat# 120568
pLEX-FHH-NRAS-IRES-Puro	This paper	Addgene Cat# 120569
pLEX-FHH-NRAS^{Q61K}-IRES-Puro	This paper	Addgene Cat# 120570
pLEX-FHH-NRAS$^{Q61K/T35A}$-IRES-Puro	This paper	Addgene Cat# 120571
pLEX-FHH-NRAS$^{Q61K/E37A}$-IRES-Puro	This paper	Addgene Cat# 120572
pLEX-FHH-NRAS$^{Q61K/Y40A}$-IRES-Puro	This paper	Addgene Cat# 120573
pLEX-FLAG-NRAS-IRES-Puro	This paper	Addgene Cat# 120574
pLEX-FLAG-NRAS^{Q61K}-IRES-Puro	This paper	Addgene Cat# 120575
pLEX-FLAG-RHEB-IRES-Puro	This paper	Addgene Cat# 120576
pMSCV mSin1.1 HA	Addgene	Cat# 12582
pcDNA3-Flag mTOR wt	Addgene	Cat# 26603
MGC Human RAF1 Sequence-Verified cDNA Clone ID: 3904404	Dharmacon	Cat# MHS6278-202756888
pLEX-MAPKAP1.1-FHH-IRES-Puro	This paper	Addgene Cat# 120705
pLEX-MAPKAP1^{Del}-FHH-IRES-Puro	This paper	Addgene Cat# 120706
pLentiGuide	Addgene	Cat# 117986
pLEX_Cas9	Addgene	Cat# 117987

REAGENT or RESOURCE	SOURCE	IDENTIFIER
pRRL Luciferase	This paper	Addgene Cat# 120798
pLEX-Frb:Akt2-IRES-Hygromycin	This paper	Addgene Cat# 120713
pLEX-FKBP-Localizer-Blasticidin	This paper	Addgene Cat# 120714-18, 120723
pLEX-FHH-Raf1^{RBD} (AA1-149)	This paper	Addgene Cat# 120707
pLEX-FHH-MTOR^{KinaseDomain} (AA1967-2549)	This paper	Addgene Cat# 120708
pLEX-FHH-MTOR^{HEAT} (AA1-409)	This paper	Addgene Cat# 120709
pLEX-FHH-MAPKAP1^{RBD} (AA279-353)	This paper	Addgene Cat# 120710
pLEX-FHH-MAPKAP1^{RBD}/Triple Mutant (AA279-353; K307A,K310A,R312L)	This paper	Addgene Cat# 120711
Software and Algorithms		
Preview	Protein Metrics	N/A
Byonic v2.6.49 or v2.14.27	Protein Metrics	N/A
Byologic	Protein Metrics	N/A
SAINT (Significance Analysis of INTeractome)	Choi et al., 2011	www.crapome.org
Cytoscape (v3.1.1)		www.cytoscape.org
MatLab	MathWorks	
STRING	Szklarczyk et al., 2015	string-db.org
Enrichr	Chen et al., 2013	http://amp.pharm.mssm.edu/Enrichr/
Bowtie	Langmead et al., 2009	http://bowtie-bio.sourceforge.net/index.shtml
MAGeCK	Li et al., 2014	https://sourceforge.net/projects/mageck/
Image Studio Lite	LI-COR	https://www.licor.com/bio/products/software/image_studio_lite/
GraphPad Prism 7.0d Software	GraphPad Software, Inc.	www.graphpad.com
Fiji (ImageJ)	Schindelin et al., 2012	fiji.sc
TopHat2	Kim et al., 2013	http://ccb.jhu.edu/software/tophat
CuffDiff2	Trapnell et al., 2013	https://github.com/cole-trapnell-lab/cufflinks
GSEA	Broad Institute	http://software.broadinstitute.org/gsea
LivingImage	Caliper LifeSciences	N/A
MO.Control Software v1.5.3	Nanotemper Technologies	N/A
MO.Affinity Analysis Software v2.2.7	Nanotemper Technologies	N/A
Other		
Immobilon-FL PVDF Membrane	Millipore Sigma	Cat# IPFL00010
Odyssey® Blocking Buffer (PBS)	LICOR	Cat# 927-4000
Monolith NT.115 Premium Capillaries	Nanotemper Technologies	Cat# MO-K025
Lysing Matrix D	MP Biomedicals	Cat# 116913500

Supplementary Material

Refer to Web version on PubMed Central for supplementary material.

ACKNOWLEDGMENTS

We thank A. Oro, H. Chang, and J. Sage as well as Z. Siprashvili and V. Lopez-Pajares, for presubmission review and comments; C. Adams, R. Leib, K. Singhal and Vincent Coates Foundation Mass Spectrometry Laboratory for mass spectrometry data acquisition and analysis. This work was supported by the USVA Office of Research and Development and by the NIH/NIAMS grant AR43799 and NIH/NCI grant CA142635 to P.A.K. The Stanford Cancer Institute Proteomics/Mass Spectrometry Shared Resource was supported in part by NIH/NCRR grants P30 CA124435 and S10RR027425.

REFERENCES

Barnard D, Diaz B, Hettich L, Chuang E, Zhang XF, Avruch J, and Marshall M (1995). Identification of the sites of interaction between c-Raf-1 and Ras-GTP. Oncogene 10, 1283–1290. [PubMed: 7731678]

Benavides-Serrato A, Lee J, Holmes B, Landon KA, Bashir T, Jung ME, Lichtenstein A, and Gera J (2017). Specific blockade of Rictor-mTOR association inhibits mTORC2 activity and is cytotoxic in glioblastoma. PLoS One 12, e0176599. [PubMed: 28453552]

Cameron AJ, Linch MD, Saurin AT, Escribano C, and Parker PJ (2011). mTORC2 targets AGC kinases through Sin1-dependent recruitment. Biochem J 439, 287–297. [PubMed: 21806543]

Chen B, Gilbert LA, Cimini BA, Schnitzbauer J, Zhang W, Li GW, Park J, Blackburn EH, Weissman JS, Qi LS, et al. (2013a). Dynamic imaging of genomic loci in living human cells by an optimized CRISPR/Cas system. Cell 155, 1479–1491. [PubMed: 24360272]

Chen EY, Tan CM, Kou Y, Duan Q, Wang Z, Meirelles GV, Clark NR, and Ma'ayan A (2013b). Enrichr: interactive and collaborative HTML5 gene list enrichment analysis tool. BMC Bioinformatics 14, 128. [PubMed: 23586463]

Choi H, Larsen B, Lin ZY, Breitkreutz A, Mellacheruvu D, Fermin D, Qin ZS, Tyers M, Gingras AC, and Nesvizhskii AI (2011). SAINT: probabilistic scoring of affinity purification-mass spectrometry data. Nat Methods 8, 70–73. [PubMed: 21131968]

Dimova DK, and Dyson NJ (2005). The E2F transcriptional network: old acquaintances with new faces. Oncogene 24, 2810–2826. [PubMed: 15838517]

Dingar D, Kalkat M, Chan PK, Srikumar T, Bailey SD, Tu WB, Coyaud E, Ponzielli R, Kolyar M, Jurisica I, et al. (2015). BioID identifies novel c-MYC interacting partners in cultured cells and xenograft tumors. J Proteomics 118, 95–111. [PubMed: 25452129]

Driscoll DR, Karim SA, Sano M, Gay DM, Jacob W, Yu J, Mizukami Y, Gopinathan A, Jodrell DI, Evans TR, et al. (2016). mTORC2 Signaling Drives the Development and Progression of Pancreatic Cancer. Cancer Res 76, 6911–6923. [PubMed: 27758884]

Ebner M, Sinkovics B, Szczygiel M, Ribeiro DW, and Yudushkin I (2017). Localization of mTORC2 activity inside cells. J Cell Biol 216, 343–353. [PubMed: 28143890]

Elias JE, and Gygi SP (2007). Target-decoy search strategy for increased confidence in large-scale protein identifications by mass spectrometry. Nat Methods 4, 207–214. [PubMed: 17327847]

Estrach S, Lee SA, Boulter E, Pisano S, Errante A, Tissot FS, Cailleteau L, Pons C, Ginsberg MH, and Feral CC (2014). CD98hc (SLC3A2) loss protects against ras-driven tumorigenesis by modulating integrin-mediated mechanotransduction. Cancer Res 74, 6878–6889. [PubMed: 25267066]

Garcia-Martinez JM, and Alessi DR (2008). mTOR complex 2 (mTORC2) controls hydrophobic motif phosphorylation and activation of serum- and glucocorticoid-induced protein kinase 1 (SGK1). Biochem J 416, 375–385. [PubMed: 18925875]

Goldfinger LE, Ptak C, Jeffery ED, Shabanowitz J, Han J, Haling JR, Sherman NE, Fox JW, Hunt DF, and Ginsberg MH (2007). An experimentally derived database of candidate Ras-interacting proteins. J Proteome Res 6, 1806–1811. [PubMed: 17439166]

Guertin DA, and Sabatini DM (2007). Defining the role of mTOR in cancer. Cancer Cell 12, 9–22. [PubMed: 17613433]

Gysin S, Salt M, Young A, and McCormick F (2011). Therapeutic strategies for targeting ras proteins. Genes Cancer 2, 359–372. [PubMed: 21779505]

Haigis KM (2017). KRAS Alleles: The Devil Is in the Detail. Trends Cancer 3, 686–697. [PubMed: 28958387]

Heikamp EB, Patel CH, Collins S, Waickman A, Oh MH, Sun IH, Illei P, Sharma A, Naray-Fejes-Toth A, Fejes-Toth G, et al. (2014). The AGC kinase SGK1 regulates TH1 and TH2 differentiation downstream of the mTORC2 complex. Nat Immunol 15, 457–464. [PubMed: 24705297]

Hernandez-Valladares M, and Prior IA (2015). Comparative proteomic analysis of compartmentalised Ras signalling. Sci Rep-Uk 5.

Karnoub AE, and Weinberg RA (2008). Ras oncogenes: split personalities. Nat Rev Mol Cell Biol 9, 517–531. [PubMed: 18568040]

Khanna A, Lotfi P, Chavan AJ, Montano NM, Bolourani P, Weeks G, Shen Z, Briggs SP, Pots H, Van Haastert PJ, et al. (2016). The small GTPases Ras and Rap1 bind to and control TORC2 activity. Sci Rep 6, 25823. [PubMed: 27172998]

Khosravi-Far R, White MA, Westwick JK, Solski PA, Chrzanowska-Wodnicka M, Van Aelst L, Wigler MH, and Der CJ (1996). Oncogenic Ras activation of Raf/mitogen-activated protein kinase-independent pathways is sufficient to cause tumorigenic transformation. Mol Cell Biol 16, 3923–3933. [PubMed: 8668210]

Kim D, Pertea G, Trapnell C, Pimentel H, Kelley R, and Salzberg SL (2013). TopHat2: accurate alignment of transcriptomes in the presence of insertions, deletions and gene fusions. Genome Biol 14, R36. [PubMed: 23618408]

Kim DI, and Roux KJ (2016). Filling the Void: Proximity-Based Labeling of Proteins in Living Cells. Trends Cell Biol 26, 804–817. [PubMed: 27667171]

Kim LC, Cook RS, and Chen J (2016). mTORC1 and mTORC2 in cancer and the tumor microenvironment. Oncogene.

Langmead B, Trapnell C, Pop M, and Salzberg SL (2009). Ultrafast and memory-efficient alignment of short DNA sequences to the human genome. Genome Biol 10, R25. [PubMed: 19261174]

Laplante M, and Sabatini DM (2012). mTOR signaling in growth control and disease. Cell 149, 274–293. [PubMed: 22500797]

Li W, Xu H, Xiao T, Cong L, Love MI, Zhang F, Irizarry RA, Liu JS, Brown M, and Liu XS (2014). MAGeCK enables robust identification of essential genes from genome-scale CRISPR/Cas9 knockout screens. Genome Biol 15, 554. [PubMed: 25476604]

Liu P, Gan W, Chin YR, Ogura K, Guo J, Zhang J, Wang B, Blenis J, Cantley LC, Toker A, et al. (2015). PtdIns(3,4,5)P3-Dependent Activation of the mTORC2 Kinase Complex. Cancer Discov 5, 1194–1209. [PubMed: 26293922]

Long X, Lin Y, Ortiz-Vega S, Yonezawa K, and Avruch J (2005). Rheb binds and regulates the mTOR kinase. Curr Biol 15, 702–713. [PubMed: 15854902]

Nan X, Tamguney TM, Collisson EA, Lin LJ, Pitt C, Galeas J, Lewis S, Gray JW, McCormick F, and Chu S (2015). Ras-GTP dimers activate the Mitogen-Activated Protein Kinase (MAPK) pathway. Proc Natl Acad Sci U S A 112, 7996–8001. [PubMed: 26080442]

Oh WJ, and Jacinto E (2011). mTOR complex 2 signaling and functions. Cell Cycle 10, 2305–2316. [PubMed: 21670596]

Pacold ME, Suire S, Perisic O, Lara-Gonzalez S, Davis CT, Walker EH, Hawkins PT, Stephens L, Eccleston JF, and Williams RL (2000). Crystal structure and functional analysis of Ras binding to its effector phosphoinositide 3-kinase gamma. Cell 103, 931–943. [PubMed: 11136978]

Papke B, and Der CJ (2017). Drugging RAS: Know the enemy. Science 355, 1158–1163. [PubMed: 28302824]

Patricelli MP, Janes MR, Li LS, Hansen R, Peters U, Kessler LV, Chen Y, Kucharski JM, Feng J, Ely T, et al. (2016). Selective Inhibition of Oncogenic KRAS Output with Small Molecules Targeting the Inactive State. Cancer Discov 6, 316–329. [PubMed: 26739882]

Prior IA, Lewis PD, and Mattos C (2012). A comprehensive survey of Ras mutations in cancer. Cancer Res 72, 2457–2467. [PubMed: 22589270]

Pylayeva-Gupta Y, Grabocka E, and Bar-Sagi D (2011). RAS oncogenes: weaving a tumorigenic web. Nat Rev Cancer 11, 761–774. [PubMed: 21993244]

Rodriguez-Viciana P, Warne PH, Vanhaesebroeck B, Waterfield MD, and Downward J (1996). Activation of phosphoinositide 3-kinase by interaction with Ras and by point mutation. EMBO J 15, 2442–2451. [PubMed: 8665852]

Roux KJ, Kim DI, and Burke B (2013). BioID: a screen for protein-protein interactions. Curr Protoc Protein Sci 74, Unit 19 23.

Roux KJ, Kim DI, Raida M, and Burke B (2012). A promiscuous biotin ligase fusion protein identifies proximal and interacting proteins in mammalian cells. J Cell Biol 196, 801–810. [PubMed: 22412018]

Sanjana NE, Shalem O, and Zhang F (2014). Improved vectors and genome-wide libraries for CRISPR screening. Nat Methods 11, 783–784. [PubMed: 25075903]

Sarbassov DD, Guertin DA, Ali SM, and Sabatini DM (2005). Phosphorylation and regulation of Akt/PKB by the rictor-mTOR complex. Science 307, 1098–1101. [PubMed: 15718470]

Schindelin J, Arganda-Carreras I, Frise E, Kaynig V, Longair M, Pietzsch T, Preibisch S, Rueden C, Saalfeld S, Schmid B, et al. (2012). Fiji: an open-source platform for biological-image analysis. Nat Methods 9, 676–682. [PubMed: 22743772]

Schroder WA, Buck M, Cloonan N, Hancock JF, Suhrbier A, Sculley T, and Bushell G (2007). Human Sin1 contains Ras-binding and pleckstrin homology domains and suppresses Ras signalling. Cell Signal 19, 1279–1289. [PubMed: 17303383]

Shankar S, Pitchiaya S, Malik R, Kothari V, Hosono Y, Yocum AK, Gundlapalli H, White Y, Firestone A, Cao X, et al. (2016). KRAS Engages AGO2 to Enhance Cellular Transformation. Cell Rep 14, 1448–1461. [PubMed: 26854235]

Shevchenko A, Tomas H, Havlis J, Olsen JV, and Mann M (2006). In-gel digestion for mass spectrometric characterization of proteins and proteomes. Nat Protoc 1, 2856–2860. [PubMed: 17406544]

Stephen AG, Esposito D, Bagni RK, and McCormick F (2014). Dragging ras back in the ring. Cancer Cell 25, 272–281. [PubMed: 24651010]

Stokoe D, and McCormick F (1997). Activation of c-Raf-1 by Ras and Src through different mechanisms: activation in vivo and in vitro. EMBO J 16, 2384–2396. [PubMed: 9171352]

Sydor JR, Engelhard M, Wittinghofer A, Goody RS, and Herrmann C (1998). Transient kinetic studies on the interaction of ras and the Ras-binding domain of c-Raf-1 reveal rapid equilibration of the complex. Biochemistry 37, 14292–14299. [PubMed: 9760267]

Szklarczyk D, Franceschini A, Wyder S, Forslund K, Heller D, Huerta-Cepas J, Simonovic M, Roth A, Santos A, Tsafou KP, et al. (2015). STRING v10: protein-protein interaction networks, integrated over the tree of life. Nucleic Acids Res 43, D447–452. [PubMed: 25352553]

Tatebe H, Morigasaki S, Murayama S, Zeng CT, and Shiozaki K (2010). Rab-family GTPase regulates TOR complex 2 signaling in fission yeast. Curr Biol 20, 1975–1982. [PubMed: 21035342]

Trapnell C, Hendrickson DG, Sauvageau M, Goff L, Rinn JL, and Pachter L (2013). Differential analysis of gene regulation at transcript resolution with RNA-seq. Nat Biotechnol 31, 46–53. [PubMed: 23222703]

Varnaite R, and MacNeill SA (2016). Meet the neighbors: Mapping local protein interactomes by proximity-dependent labeling with BioID. Proteomics 16, 2503–2518. [PubMed: 27329485]

Walker EH, Perisic O, Ried C, Stephens L, and Williams RL (1999). Structural insights into phosphoinositide 3-kinase catalysis and signalling. Nature 402, 313–320. [PubMed: 10580505]

Wang MT, Holderfield M, Galeas J, Delrosario R, To MD, Balmain A, and McCormick F (2015). K-Ras Promotes Tumorigenicity through Suppression of Non-canonical Wnt Signaling. Cell 163, 1237–1251. [PubMed: 26590425]

Wang T, Yu H, Hughes NW, Liu B, Kendirli A, Klein K, Chen WW, Lander ES, and Sabatini DM (2017). Gene Essentiality Profiling Reveals Gene Networks and Synthetic Lethal Interactions with Oncogenic Ras. Cell 168, 890–903 e815 [PubMed: 28162770]

Yang H, Jiang X, Li B, Yang HJ, Miller M, Yang A, Dhar A, and Pavletich NP (2017). Mechanisms of mTORC1 activation by RHEB and inhibition by PRAS40. Nature 552, 368–373. [PubMed: 29236692]

Yao CA, Ortiz-Vega S, Sun YY, Chien CT, Chuang JH, and Lin Y (2017). Association of mSin1 with mTORC2 Ras and Akt reveals a crucial domain on mSin1 involved in Akt phosphorylation. Oncotarget.

Highlights

- Proximity proteomics of WT and MT Ras finds new interactors and cellular functions
- Proteomic integration with CRISPR genetics identifies mTOR as Ras proximal protein
- Mutant Ras directly binds and activates mTORC2
- Disrupting the MT Ras-mTORC2 interaction impedes Ras tumorigenesis in vivo

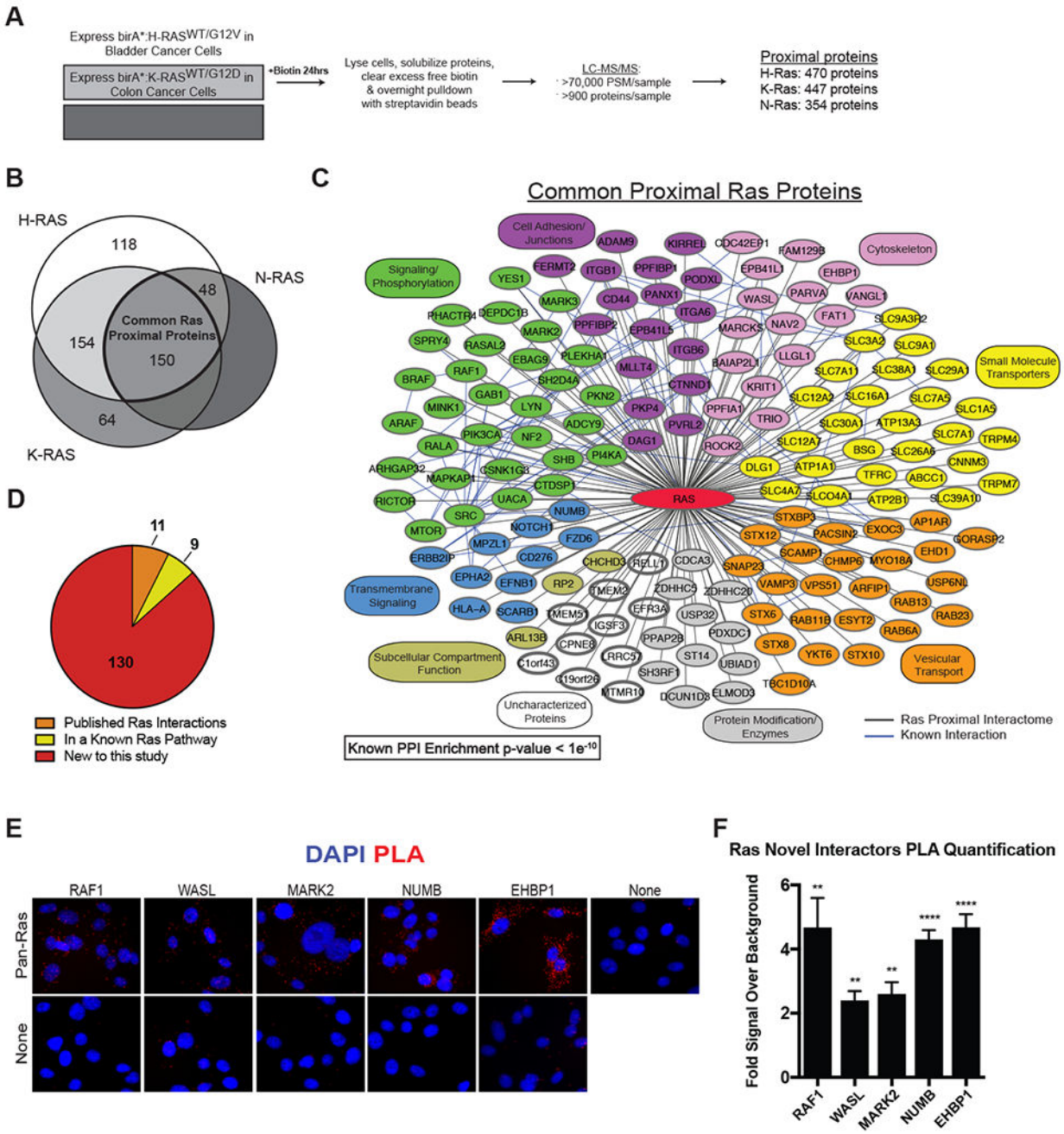

Figure 1. H-, K-, N-Ras-proximal Proteins in Human Cancer Cells.

(A) Proximity-dependent protein labeling (BioID) experimental workflow. LC-MS/MS, Liquid chromatography tandem-mass spectrometry. PSM, peptide-spectrum match. **(B)** Overlap of Ras-proximal proteins identified in each birA*:Ras isoform interactome. SAINT probability score ≥ 0.8; fold change ≥ 4 over birA* control. **(C)** Interaction network of 150 proteins common to all Ras isoforms. P-value calculated via STRING (Szklarczyk et al., 2015). **(D)** New and known interactors within 150 common proteins. **(E)** PLA in MT *NRAS* MM415 melanoma cells of endogenous Ras interactome candidates with endogenous Ras

protein; punctate signal as reported (red) (Patricelli et al., 2016), nuclei (blue). None is single antibody control. Scale bar, 20μm. **(F)** Quantification of the PLA analysis shown in (E). n= 4-5 fields per sample, 1 experiment; mean ± SEM. **p< 0.01, ****p< 0.0001 (unpaired two-sided t-test to single antibody controls). See also Figures S1 and S2, and Table S1.

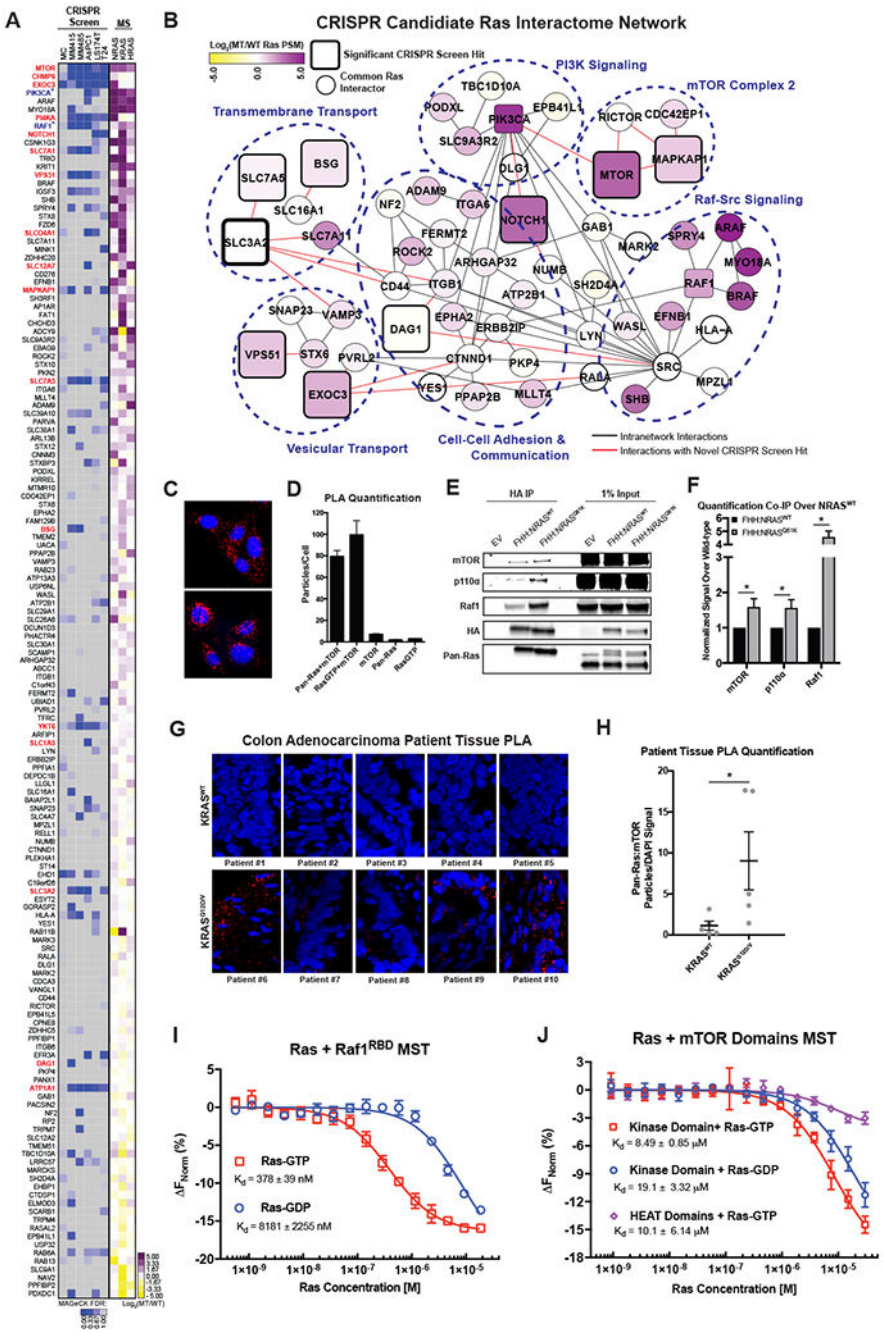

Figure 2. Multi-Cell Line CRISPR Screen of Ras Proximal Proteins.

(A) A two-week growth CRISPR screen of 150 common Ras-proximal proteins in diploid primary human melanocytes (MC) and 5 MT Ras cell lines. Left heatmap negative selection FDR values (FDR ≤ 0.18) in each cell type by the MAGeCK algorithm (Li et al., 2014). The right heatmap relative enrichment MT vs WT Ras in mass spectrometry data for each Ras isoform; new proteins (red), known proteins (*). Ranked by combined FDR and $\log_2$(PSM MT/WT Ras) score. **(B)** Common Ras-proximal interacting protein-protein network based on candidates with ≥1 database interaction with another common interactor. Large squares

are novel and small squares are known interactors. **(C)** PLA in MT *NRAS* MM415 melanoma cells with endogenous mTOR and Pan-Ras or Ras:GTP; interaction (red), nuclei (blue). Scale bar, 20 μm. **(D)** Quantification of PLA analysis in (C). n=8-10 fields/condition. **(E)** Western blot of HA co-immunoprecipitation of empty vector (EV), FLAG-HA-6xHIS tagged $NRAS^{WT}$ or FHH: $NRAS^{Q61K}$ with endogenous mTOR, p110α and Raf1 in wild-type RAS CHL-1 cells. **(F)** Quantification of HA co-IP experiments as in (E). Values are normalized to HA pulldown signal and relative to $NRAS^{WT}$ signal, n= 6 (Wilcoxon Signed Rank Test). **(G)** PLA in genotyped human colorectal adenocarcinomas with endogenous Pan-Ras and mTOR. Scale bar, 20 μm. **(H)** Quantification of PLA analysis in (G). Each dot represents median signal per patient. n=5 patients/genotype group, ≥7 images analyzed per patient (Mann-Whitney U Test). **(I)** Microscale thermophoresis with labeled FHH:$Raf1^{RBD}$ (18.2nM) with a titration series of GDP or GTPγs-loaded Ras. The binding curve is negative as the MST signal of the complex is lower than that of $Raf1^{RBD}$ alone. MST-on time of 15s, n = 3 independent replicates. **(J)** Microscale thermophoresis with labeled FHH:$mTOR^{KinaseDomain}$ and FHH:$mTOR^{HEAT}$ (23.4nM) with a titration series of GDP or GTPγs-loaded Ras. MST-on time of 2.5s, n ≥ 3 independent replicates. MST is mean ± SD. All other data mean ± SEM; *p< 0.05. See also Figures S3 and S4, Tables S2–4.

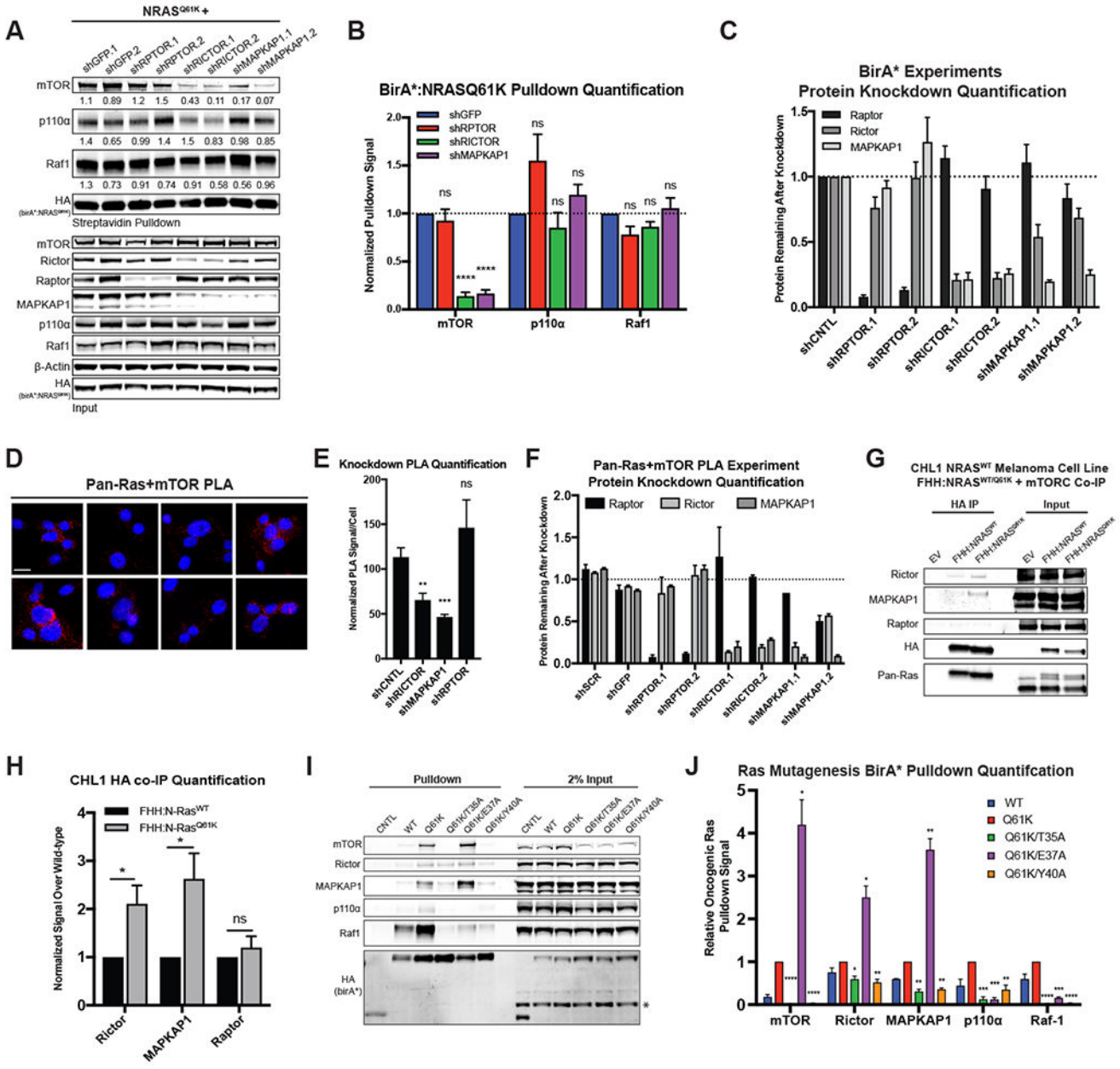

Figure 3. Oncogenic Ras Interacts with mTORC2 via the Effector Binding Domain.

(A) BioID-western blot showing mTOR protein levels in the streptavidin pulldowns of birA*:NRAS^{Q61K} with sh*GFP*, sh*RPTOR*, sh*RICTOR* or sh*MAPKAP1* with two independent hairpins in CHL-1 cells. PI3K p110α subunit, Raf1, and HA protein levels in streptavidin pulldowns are controls. Pulldown and input normalized values relative to the control shown below. **(B)** Quantification of mTOR, p110α and Raf1 protein levels in the streptavidin pulldown Normalized to HA pulldown and respective input levels and relative to shGFP mean, n=5 (unpaired two-sided t-test). **(C)** Quantification of protein remaining after knockdown compared to the average of controls for (B). **(D)** PLA in MT *NRAS* MM415 melanoma cells with endogenous Ras and mTOR with control, mTORC1 or mTORC2

component knockdown. Scale bar, 20 μm. **(E)** Quantification of PLA shown in (D). n=2 independent hairpins per knockdown. Relative to the mean of control knockdowns. (unpaired two-sided t-test). **(F)** Quantification of protein remaining after knockdown relative to mean signal of control knockdowns for PLA in (E). **(G)** Western blot of HA co-immunoprecipitation of empty vector (EV), FHH:$NRAS^{WT}$ or FHH:$NRAS^{Q61K}$ with endogenous Rictor, MAPKAP1 and Raptor in wild-type Ras CHL-1 cells. (**H)** Quantification of HA co-IP experiments as in (G). Values normalized to HA pulldown signal and relative to $NRAS^{WT}$ signal. n= 5 or 8 (Welch's two-sided t-test). **(I)** Western blot showing mTOR protein levels in the input and streptavidin pulldowns of birA* control, $NRAS^{WT}$, $NRAS^{Q61K}$ and $NRAS^{Q61K}$ Effector Domain Alanine point mutants. (*) non-specific background band. **(J)** Quantification of streptavidin pulldown protein levels as in (I). mTOR signal normalized to HA signal. All values relative to birA*: $NRAS^{Q61K}$, n=3 (Welch's two-sided t-test relative to Q61K). All graphed data are mean ± SEM. *p< 0.05, **p< 0.01, ***p< 0.001, ****p< 0.0001, ns= not significant. See also Figure S5.

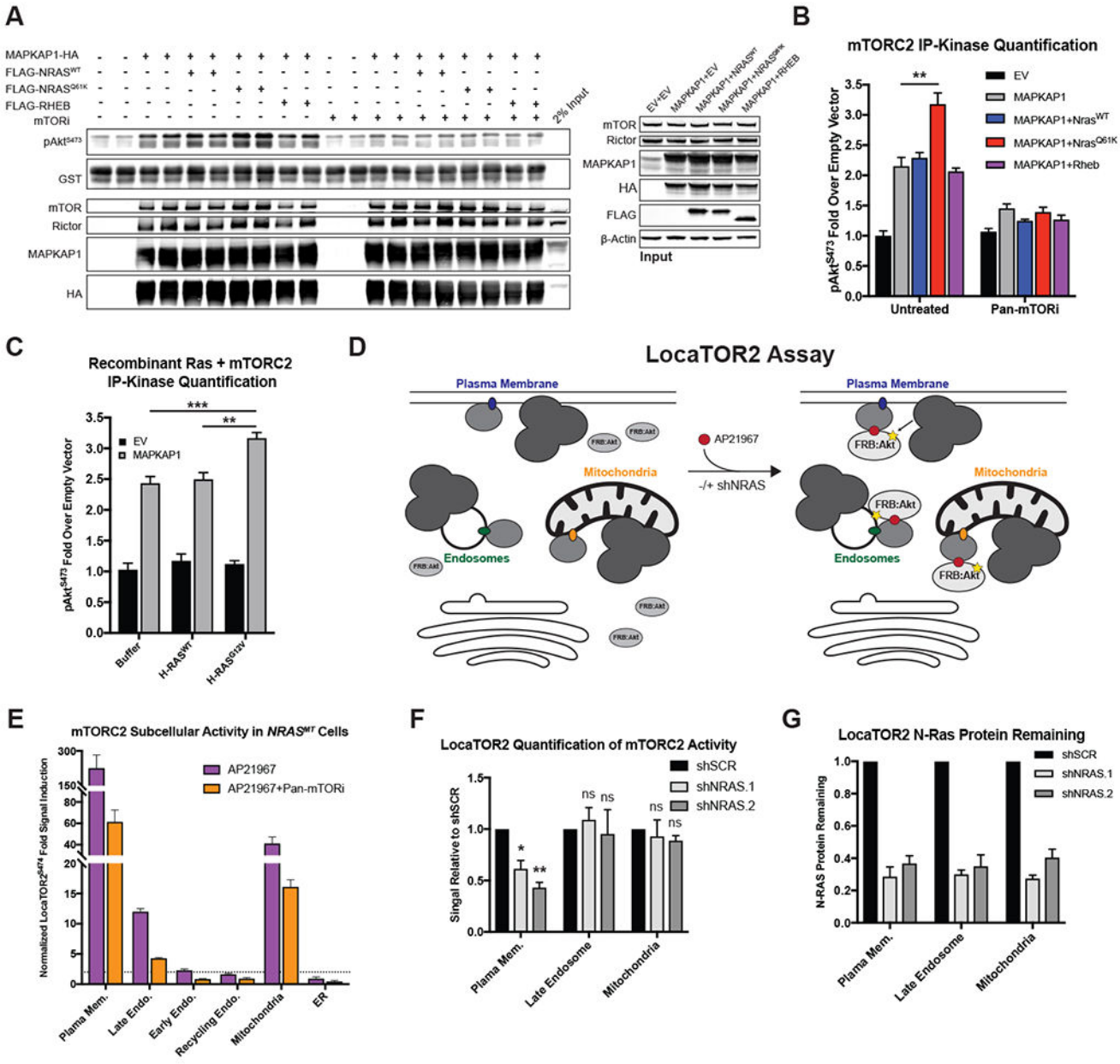

Figure 4. Oncogenic Ras Positively Regulates mTORC2 Kinase Activity.

(A) Western blot of replicate *in vitro* mTORC2 IP-kinase assays with a GST-Akt1 tail substrate. Input levels right panel. HA-tagged MAPKAP1 pulldown of mTORC2 from 293T cells co-expressing empty vector (EV) or FLAG-GTPase. 5 μM PP242 (mTORi). **(B)** Quantification of the GST normalized mTORC2 IP-kinase assay pAkt^{S473} signal, as in (A), relative to mean of the untreated EV control. n= 4-6 (unpaired two-sided t-test). **(C)** Quantification of HA IP mTORC2 kinase assay with addition of indicated recombinant GDP-loaded WT or GTPγS-loaded G12V H-Ras *in vitro* relative to EV in buffer only. n=5-6; ** $p < 0.01$, (unpaired two-sided t-test). **(D)** Diagram of the LocaTOR2 assay for subcellular compartment-specific *in vivo* mTORC2 kinase activity. **(E)** LocaTOR2-based

subcellular compartment mTORC2 activity quantified as phosphorylated Frb:Akt2^{S474} signal over untreated in MT *NRAS* MM485 melanoma cells. 500 nM KU-0063794 (Pan-mTORi). Dotted line at 2. n=2 experimental replicates. **(F)** Quantification of compartment-specific LocaTOR2 signal with shSCR or shNRAS knockdown, n=3. (Welch's two-sided t-test to respective shSCR). **(G)** Quantification of protein remaining after knockdown compared to shSCR for (F). All data are mean ± SEM. *p< 0.05, **p< 0.01, ***p< 0.001. See also Figure S6.

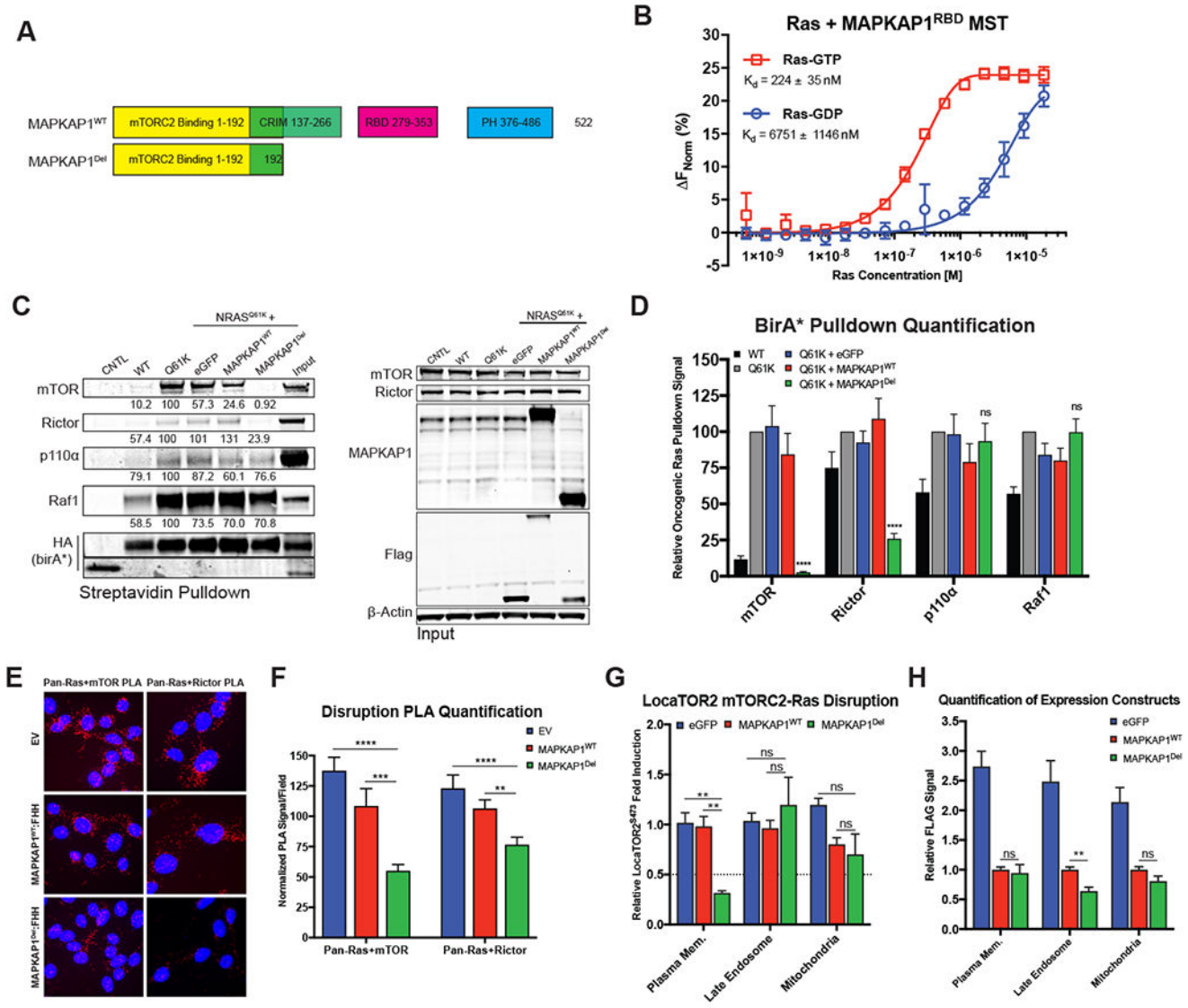

Figure 5. MAPKAP1 Binds to Ras and Modulates the Ras-mTORC2 Interaction.

(A) Schematic of full length MAPKAP1 isoform 1 wild-type (WT) and the MAPKAP1 deletion (Del) proteins with domains highlighted. CRIM, Conserved Region In The Middle. RBD, Ras Binding Domain. PH, Pleckstrin Homology. **(B)** Microscale thermophoresis of labeled FHH:MAPKAP1^{RBD} (16.8nM) with a titration series of GDP or GTPγs-loaded Ras. The binding curve is positive as the MST signal of the complex is higher than MAPKAP1^{RBD} alone. MST-on time of 5s, n = 3 independent replicates. **(C)** BioID-western blot streptavidin pulldowns and input levels for birA* control, NRAS^{WT}, NRAS^{Q61K} and NRAS^{Q61K} with FHH:eGFP, MAPKAP1^{WT}:FHH or MAPKAP1^{Del}:FHH expression in CHL-1 cells. PI3K p110α subunit, Raf-1, and HA protein pulldown are controls. Pulldown normalized signal relative to control birA*:NRAS^{Q61K} shown below. **(D)** Quantification of mTOR and Rictor protein levels in the streptavidin pulldowns normalized to HA pulldown. All values and statistical tests relative to birA*:NRAS^{Q61K}, n=6 (Welch's two-sided t-test). **(E)** PLA with endogenous Pan-Ras and mTOR or Rictor in MT *NRAS* MM485 melanoma

cells. Scale bar, 20 μm. **(F)** PLA quantification in (E). n=3 independent experiments, 6-8 fields analyzed per condition per experiment (unpaired two-sided t-test). EV, empty vector. **(G)** Quantification of LocaTOR2 experiments with FHH:eGFP, MAPKAP1^{WT}:FHH or MAPKAP1^{Del}:FHH expression. All values relative to average of FHH:eGFP and MAPKAP1^{WT}:FHH fold induction; n=3 (unpaired two-sided t-test). **(H)** Quantification of FHH:eGFP, MAPKAP1^{WT}:FHH and MAPKAP1^{Del}:FHH expression relative to MAPKAP1^{WT}:FHH for all experiments graphed in (G). **p< 0.01, ***p< 0.001, ****p< 0.0001, and ns= not significant; all bar graphed data mean ± SEM. MST data are mean ± SD. See also Figure S6 and Table S4.

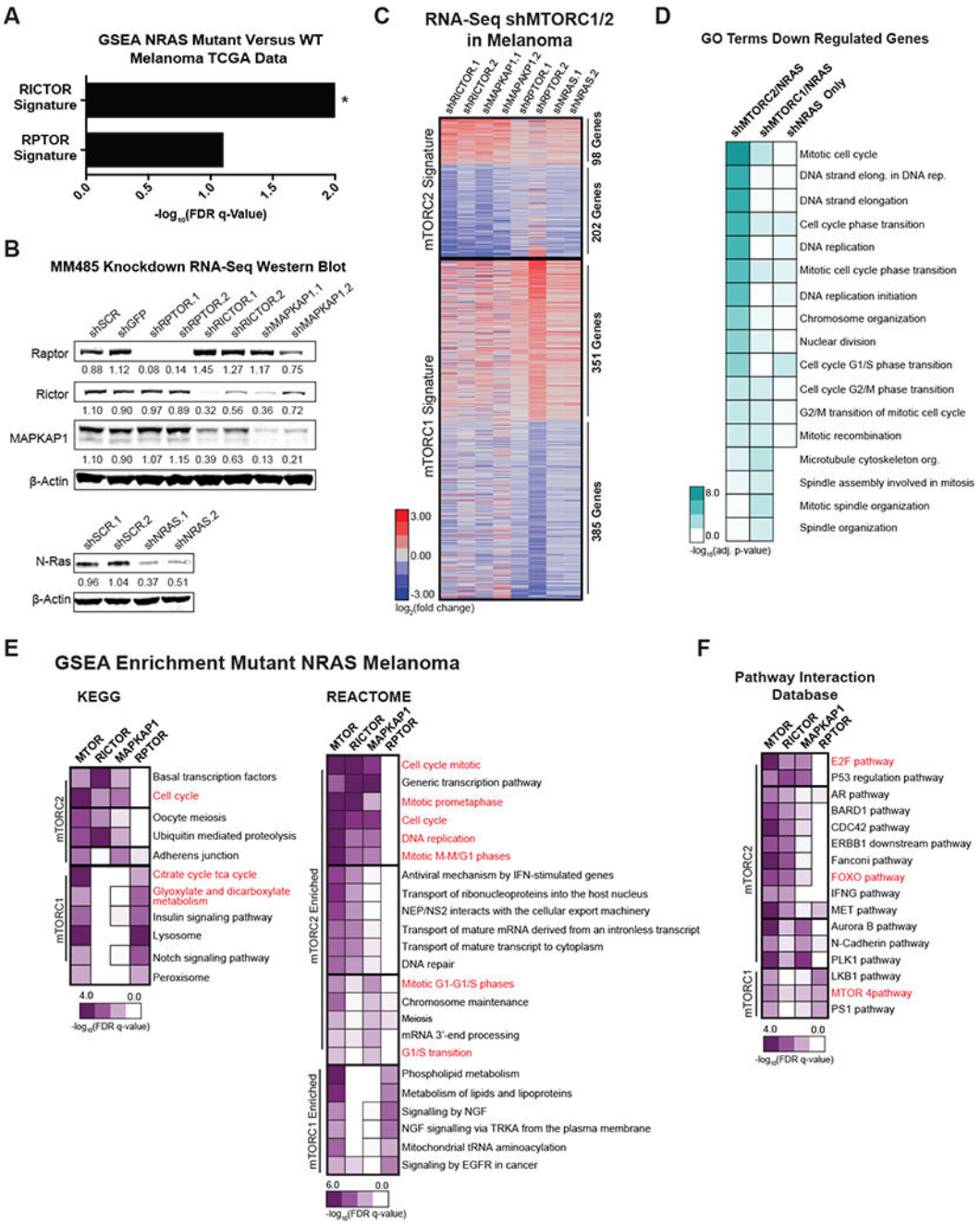

Figure 6. Oncogenic Ras with mTORC2 Regulates Cell Cycle Genes.

(A) Gene set enrichment analysis (GSEA) of *RICTOR* (Normalized enrichment score = −1.20) and *RPTOR* (NES= −1.30) knockdown signatures from primary human melanocytes comparing $NRAS^{WT}$ versus $NRAS^{MT}$ melanoma patient sample TCGA RNA expression data. *p< 0.05. **(B)** Western blot of protein remaining in control, *RPTOR, RICTOR, MAPKAP1,* and *NRAS* knockdown RNA-sequencing samples in MT *NRAS* melanoma cell line MM485. Labeled with normalized protein remaining relative to the control average. **(C)** Heat map showing log_2(fold change) in RNA-sequencing of MT *NRAS* melanoma line,

MM485, with *RICTOR, MAPKAP1, RPTOR* or *NRAS* knockdown compared to control. mTORC2 gene signature is derived from concordant genes between sh*RICTOR* and sh*MAPKAP1* samples and mTORC1 signature between sh*RPTOR* samples. **(D)** Heatmap of $-\log_{10}$(adjusted p-values) for top GO terms for NRAS-regulated shMTORC1 and shMTORC2 down regulated gene sets as labeled in (C). Unfiltered shNRAS down regulated gene set analysis for comparison. **(E)** Heatmap of $-\log_{10}$(FDR q-values) for GSEA positively enriched REACTOME or KEGG or **(F)** Pathway interaction database (PID) signatures from Molecular Signatures Database with *MTOR, RICTOR, MAPKAP1* or *RPTOR* expression as the phenotype in MT *NRAS* TCGA melanoma patient samples. Relevant signatures (red). See also Figure S7, Tables S5 and S6.

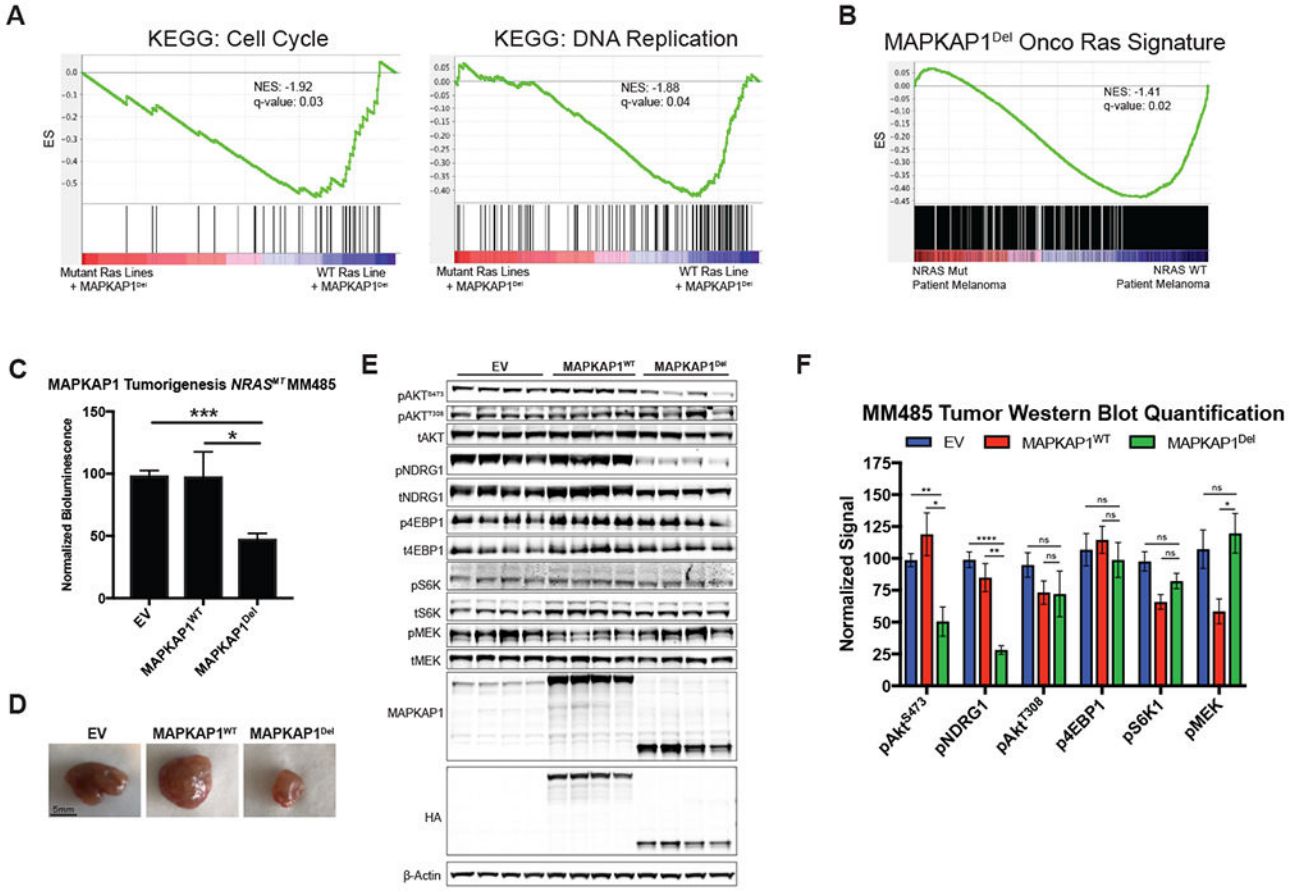

Figure 7. MAPKAP1^{Del} Alters the Oncogenic Ras Transcriptional Program and Tumorigenesis.

(A) GSEA enrichment plots of genes altered with MAPKAP1^{Del} expression in MT versus WT *NRAS* melanoma cell lines. NES, normalized enrichment score. **(B)** GSEA enrichment plot of MT *NRAS* cell line-derived MAPKAP1^{Del} gene signature in MT versus WT *NRAS* TCGA melanoma patient samples. **(C)** Day 0 normalized bioluminescence for empty vector (EV), MAPKAP1^{WT}:FHH or MAPKAP1^{Del}:FHH expressing MM485 MT *NRAS* melanoma tumors at final time point. n=4 mice/group, one experiment; (unpaired two-sided t-test). **(D)** Representative images of tumors from experiment in (C). **(E)** Western blot of EV, MAPKAP1^{WT}:FHH, or MAPKAP1^{Del}:FHH-expressing MM485 tumors. **(F)** Quantification of western blots shown in (E) normalized to total protein. (unpaired two-sided t-test). All data are mean ± SEM. *p< 0.05, **p< 0.01, ***p< 0.001, ****p< 0.0001, and ns= not significant. See also Figure S7, Table S6.

REAGENT or RESOURCE	SOURCE	IDENTIFIER
Antibodies		
Ki67	ThermoFisher	Cat# RM-9106; RRID:AB_2341197
Pan-Ras (C-4) (PLA and western)	Santa Cruz Biotechnology	Cat# sc-166691; RRID:AB_2154229
Raf-1 (C12) (PLA and western)	Santa Cruz Biotechnology	Cat# sc-133; RRID:AB_632305
WASL	ProteinTech	Cat# 14306-1-AP; RRID:AB_10638478
MARK2	Sigma-Aldrich	Cat# HPA038790; RRID:AB_10674840
NUMB	Abcam	Cat# ab14140; RRID:AB_443023
EHBP1	ProteinTech	Cat# 17637-1-AP; RRID:AB_2097216
RAFT1	BD Transduction Laboratories	Cat# 611132; RRID:AB_398443
MTOR (PLA)	Abcam	Cat# ab2732; RRID:AB_303257
SIN1 (PLA)	Bethyl Laboratories	Cat# A300-910A; RRID:AB_661901
Raptor (PLA)	ProteinTech	Cat# 20984-1-AP; RRID:AB_11182390
MTOR (western)	Cell Signaling Technologies	Cat# 2972; RRID:AB_330978
P13 Kinase p110α	Cell Signaling Technologies	Cat# 4249; RRID:AB_2165248
HA-tag (C29F4) (Rabbit)	Cell Signaling Technologies	Cat# 3724; RRID:AB_1549585
HA-tag (Mouse)	Abcam	Cat# ab130275; RRID:AB_11156884
HRAS (C-20)	Santa Cruz Biotechnology	Cat# sc-520; RRID:AB_631670
NRAS (C-20)	Santa Cruz Biotechnology	Cat# sc-519; RRID:AB_632073
β-Actin	Sigma-Aldrich	Cat# A1978; RRID:AB_476692
Rictor (PLA and western)	Bethyl Laboratories	Cat# A300-459A; RRID:AB_2179967
MAPKAP1 (western)	ProteinTech	Cat# 15463-1-AP; RRID:AB_10598466
Raptor	Bethyl Laboratories	Cat# A300-553A; RRID:AB_2130793
Phospho-AKT (Ser473)	Cell Signaling Technologies	Cat# 4060; RRID:AB_2315049
Phospho-AKT (Thr308)	Cell Signaling Technologies	Cat# 13038; RRID:AB_2629447
Akt(pan)	Cell Signaling Technologies	Cat# 2920; RRID:AB_1147620
Phospho-4E-BP1 (Thr37/46)	Cell Signaling Technologies	Cat# 2855; RRID:AB_560835
4E-BP1	Cell Signaling Technologies	Cat# 9644; RRID:AB_2097841
Phospho-NDRG1 (Thr346)	Cell Signaling Technologies	Cat# 5482; RRID:AB_10693450
NDRG1	Cell Signaling Technologies	Cat# 9485; RRID:AB_2721143
NDRG1	ProteinTech	Cat# 26902-1-AP
Phospho-p70 S6 Kinase (Thr389)	Cell Signaling Technologies	Cat# 9205; RRID:AB_330944
p70 S6 Kinase	Cell Signaling Technologies	Cat# 2708; RRID:AB_390722
Living Colors mCherry	Takara	Cat# 632543; RRID:AB_2307319
Phospho-MEK1/2 (Ser217/221) (41G9)	Cell Signaling	Cat# 9154; RRID:AB_2138017
MEK1/2	Cell Signaling	Cat# 9122; RRID:AB_823567
Phospho-p44/42 MAPK (Erk1/2) (Thr202/Tyr204) (197G2)	Cell Signaling	Cat# 4377; RRID:AB_331775
p44/42 MAPK (Erk1/2) (3A7)	Cell Signaling	Cat# 9107; RRID:AB_2235073
GST (26H1)	Cell Signaling	Cat# 2624; RRID:AB_2189875

REAGENT or RESOURCE	SOURCE	IDENTIFIER
FLAG M2	Sigma-Aldrich	Cat# F1804; RRID:AB_262044
800CW Goat anti-Mouse IgG (H + L)	LI-COR	Cat# 926-32210; RRID:AB_621842
800CW Goat anti-Rabbit IgG (H + L)	LI-COR	Cat# 926-32211; RRID:AB_621843
680RD Goat anti-Mouse IgG (H + L)	LI-COR	Cat# 926-68070; RRID:AB_10956588
Duolink In Situ PLA Probe Anti-Mouse PLUS	Millipore Sigma	Cat# DUO92001
Duolink In Situ PLA Probe Anti-Rabbit MINUS	Millipore Sigma	Cat# DUO92005
Goat anti-mouse IgG (H+L)	Thermo Fisher Scientific	Cat# A21422; RRID:AB_2535844
Goat anti-Rabbit IgG (H+L)	Thermo Fisher Scientific	Cat# A11008; RRID:AB_143165
Bacterial and Virus Strains		
Biological Samples		
Colorectal adenocarcinoma tissue specimens	Asterand Biosceinces (BioIVT)	N/A
Discard Surgical Skin Tissue	Stanford University	N/A
Chemicals, Peptides, and Recombinant Proteins		
Medium 254	Thermo Fisher Scientific	Cat# M254500
Human Melanocyte Growth Supplement (HMGS)	Thermo Fisher Scientific	Cat# S0025
Lipofectamine 200	Thermo Fisher Scientific	Cat# 11668019
Lenti-X Concentrator	Takara	Cat# 631232
10× Cell Lysis Buffer	Cell Signaling Technologies	Cat# 9803
cOmplete, Mini, EDTA-free Protease Inhibitor Cocktail	Millipore Sigma	Cat# 11836170001
PhosStop	Millipore Sigma	Cat# 4906837001
800CW Streptavidin	LI-COR	Cat# 926-32230
Dynabeads MyOne Streptavidin C1	Thermo Fisher Scientific	Cat# 65002
Trypsin/Lys-C Mix	Promega	Cat# V5071
ProteaseMAX	Promega	Cat# V2071
$NRAS^{Q61K}$ Human Recombinant Protein	Origene	Cat# TP701004
NRAS Human Recombinant Protein	Origene	Cat# TP302681
MAPKAP1 Human Recombinant Protein	Origene	Cat# TP311745
mTOR Human Recombinant Protein	Origene	Cat# TP320457
$KRAS^{G12D}$ Human Recombinant Protein	Origene	Cat# TP700052
$HRAS^{WT}$ Human Recombinant Protein	Origene	Cat# TP316409
$HRAS^{G12V}$ Human Recombinant Protein	Origene	Custom Production from clone Cat# RC400129
GST protein, tag-free	Millipore Sigma	Cat# SRP5348
Human KRAS full length protein	Abcam	Cat# ab90768
PI3Kγ Human Recombinant Protein	Origene	Cat# TP307790
RalGDS Human Recombinant Protein	Origene	Cat# TP316933
RAF1 Human Recombinant Protein	Origene	Cat# TP301983
MLST8 (Human) Recombinant Protein	Abnova	Cat# H00064223-P01
Akt1	Jena Bioscience	Cat# PR-325

REAGENT or RESOURCE	SOURCE	IDENTIFIER
GTP-γ-S	Abcam	Cat# ab146662
GTP-γ-S	Cytoskeleton, Inc	Cat# BS01
BS3, No-Weigh Format	Thermo Fisher Scientific	Cat# 21585
PrimeSTAR Max DNA Polymerase	Takara	Cat# R045B
Antigen Retrieval Buffer (100× Citrate Buffer pH 6.0)	Abcam	Cat# ab93678
SuperSignal West Dura Reagent	Thermo Fisher Scientific	Cat# 34075
ANTI-FLAG M2 Affinity Gel	Millipore Sigma	Cat# A2220
Amicon Ultra-0.5 mL Centrifugal Filters	Millipore Sigma	Cat# UFC501096
Colloidal Gold Total Protein Stain	Bio-Rad	Cat# 1706527
InstantBlue Protein Stain	Expedeon	Cat# ISB1L
GDP	Abcam	Cat# ab146529
Pierce Anti-HA Agarose	Thermo Fisher Scientific	Cat# 26182
Pierce Anti-HA Magnetic Beads	Thermo Fisher Scientific	Cat# 88837
Torkinib (PP242)	Selleck Chemicals	Cat# S2218
GST-Akt1tail-AA409-480	GenScript	Custom Production
H-Ras (wild-type) (human), (recombinant) [IP-Kinase]	Enzo Life Sciences	Cat# BML-SE131-0100
Recombinant H-Ras (G12V) protein (GST Tagged) [IP-Kinase]	Abcam	Cat# ab90627
AP21967 (A/C Heterodimerizer)	Takara	Cat# 635055
KU-0063794	Selleck Chemicals	Cat# S1226
BD Matrigel Matrix	BD Biosciences	Cat# 354234
H-Ras protein: His tagged: human wild type (MST)	Cytoskeleton, Inc	Cat# RS01
Critical Commercial Assays		
MycoAlert Mycoplasma Detection kit	Lonza	Cat# LT07-318
In-Fusion HD Cloning Plus	Takara	Cat# 638909
Pierce BCA Protein Assay Kit	Thermo Fisher Scientific	Cat# 23225
Colloidal Blue Staining Kit	Thermo Fisher Scientific	Cat# LC6025
DNeasy Blood and Tissue Isolation Kit	QIAGEN	Cat# 69506
OneStep PCR Inhibitor Removal Kit	Zymo	Cat# D6030
NucleoSpin Gel and PCR Clean-Up	Takara	Cat# 740609.250
Duolink In Situ Detection Reagents Orange	Millipore Sigma	Cat# DUO92007
Monolith His-Tag Labeling Kit RED-tris-NTA	Nanotemper Technologies	Cat# MO-L008
TruSeq RNA Library Prep Kit v2	Illumina	Cat# RS-122-2001
CellTiter-Blue Cell Viability Assay	Promega	Cat# G8080
Deposited Data		
Cell Line RNA Sequencing Data	This paper	Sequence Read Archive: SRP156923
HT-1376 RNA Sequencing Data	Cancer Cell Line Encylopedia	https://portals.broadinstitute.org/ccle/data
Caco-2 RNA Sequencing Data	Gene Expression Omnibus (GEO) repository	GSE48603
Ras Proximity Proteomics Peptide Counts	This paper	Table S1

REAGENT or RESOURCE	SOURCE	IDENTIFIER
CRISPR Screen Unique Guide Counts	This paper	Table S2
Crosslinking Mass Spectrometry Data	This paper	Table S4
Primary Melanocyte Gene Level Expression Data	This paper	Table S5
Mutation and expression analysis of melanoma.	Cancer Genome Atlas Research Network	https://portal.gdc.cancer.gov/projects/TCGA-SKCM
Bladder carcinoma, colon adenocarcinoma & melanoma Ras allele mutations.	Catalogue of Somatic Mutations in Cancer (COSMIC) v.72	https://cancer.sanger.ac.uk/cosmic
Raw Images of Data	This study, Mendeley Data	http://dx.doi.org/10.17632/kzxnrmh7fc.1
Experimental Models: Cell Lines		
Human: CHL-1	ATCC	CRL-9446
Human: HEK-293T	Lab stock	N/A
Human: HT-1376	ATCC	CRL-1472
Human: Caco-2	ATCC	HTB-37
Human: SK-MEL-2	ATCC	HTB-68
Human: LS 174T	ATCC	CL-188
Human: BxPC-3	ATCC	CRL-1687
Human: MM415	CellBank Australia	CBA-1351
Human: MM485	CellBank Australia	CBA-1355
Human: AsPC-1	ATCC	CRL-1682
Human: DLD-1 $KRAS^{+/-}$	Horizon Discovery	HD 105-002
Human: DLD-1 $KRAS^{G13D/-}$	Horizon Discovery	HD 105-011
Human: T24	ATCC	HTB-4
Human: SK-MEL-5	ATCC	HTB-70
Human: Capan-2	ATCC	HTB-80
Primary Melanocytes	Stanford University	N/A
Experimental Models: Organisms/Strains		
Mouse: SCID Hairless Outbred (SHO) Crl:SHO-*Prkdc*^{scid}*Hr*^{hr}	Charles River Laboratories	474
Oligonucleotides		
shRNA sequences, see Table S7	This study	N/A
qPCR primers, see Table S7	This study	N/A
CRISPR Library Construction Primers, see Table S7	This study	N/A
Recombinant DNA		
pLKO.1 - TRC cloning vector (Puro). See Table S7 for shRNA sequences.	Addgene	Cat#10878
pLKO.1-blast	Addgene	Cat #26655
pLKO.1 shSCR	Addgene	Cat #17920
pLKO.1 GFP shRNA (Puro)	Addgene	Cat #30323
GIPZ Non-silencing Lentiviral shRNA Control	Dharmacon	Cat # RHS4346
GIPZ NRAS shRNA V3LHS_402088	Dharmacon	Cat # RHS4531-EG4893

REAGENT or RESOURCE	SOURCE	IDENTIFIER
GIPZ NRAS shRNA V2LHS_152358	Dharmacon	Cat # RHS4531-EG4893
GIPZ HRAS shRNA V3LHS_641012	Dharmacon	Cat# RHS4531-EG3265
GIPZ HRAS shRNA V3LHS_645806	Dharmacon	Cat# RHS4531-EG3265
LentiORF pLEX-MCS-IRES-Puro	Open Biosystems	Cat# OHS4735
pCGN N-Ras WT	Addgene	Cat# 14723
pLEX-uORF-HA-birA*-STOP-IRES-Puro	This Paper	Addgene Cat# 120558
pLEX-uORF-HA-birA*-H-Ras(wildtype)-IRES-Puro	This paper	Addgene Cat# 120559
pLEX-uORF-HA-birA*-H-Ras(G12V)-IRES-Puro	This paper	Addgene Cat# 120560
pLEX-HA-birA*-K-Ras(wildtype)-IRES-Puro	This paper	Addgene Cat# 120561
pLEX-HA-birA*-K-Ras(G12D)-IRES-Puro	This paper	Addgene Cat# 120562
pLEX-uORF-HA-birA*-N-Ras(wildtype)-IRES-Puro	This paper	Addgene Cat# 120563
pLEX-uORF-HA-birA*-N-Ras(Q61K)-IRES-Puro	This paper	Addgene Cat# 120564
pLEX-uORF-HA-birA*-N-Ras(Q61K/T35A)-IRES-Puro	This paper	Addgene Cat# 120565
pLEX-uORF-HA-birA*-N-Ras(Q61K/E37A)-IRES-Puro	This paper	Addgene Cat# 120566
pLEX-uORF-HA-birA*-N-Ras(Q61K/Y40A)-IRES-Puro	This paper	Addgene Cat# 120567
pLEX-FHH-Empty Vector-IRES-Puro	This paper	Addgene Cat# 120568
pLEX-FHH-NRAS-IRES-Puro	This paper	Addgene Cat# 120569
pLEX-FHH-NRAS^{Q61K}-IRES-Puro	This paper	Addgene Cat# 120570
pLEX-FHH-NRAS$^{Q61K/T35A}$-IRES-Puro	This paper	Addgene Cat# 120571
pLEX-FHH-NRAS$^{Q61K/E37A}$-IRES-Puro	This paper	Addgene Cat# 120572
pLEX-FHH-NRAS$^{Q61K/Y40A}$-IRES-Puro	This paper	Addgene Cat# 120573
pLEX-FLAG-NRAS-IRES-Puro	This paper	Addgene Cat# 120574
pLEX-FLAG-NRAS^{Q61K}-IRES-Puro	This paper	Addgene Cat# 120575
pLEX-FLAG-RHEB-IRES-Puro	This paper	Addgene Cat# 120576
pMSCV mSin1.1 HA	Addgene	Cat# 12582
pcDNA3-Flag mTOR wt	Addgene	Cat# 26603
MGC Human RAF1 Sequence-Verified cDNA Clone ID: 3904404	Dharmacon	Cat# MHS6278-202756888
pLEX-MAPKAP1.1-FHH-IRES-Puro	This paper	Addgene Cat# 120705
pLEX-MAPKAP1^{Del}-FHH-IRES-Puro	This paper	Addgene Cat# 120706
pLentiGuide	Addgene	Cat# 117986
pLEX_Cas9	Addgene	Cat# 117987
pRRL Luciferase	This paper	Addgene Cat# 120798
pLEX-Frb:Akt2-IRES-Hygromycin	This paper	Addgene Cat# 120713
pLEX-FKBP-Localizer-Blasticidin	This paper	Addgene Cat# 120714-18, 120723
pLEX-FHH-Raf1^{RBD} (AA1-149)	This paper	Addgene Cat# 120707
pLEX-FHH-MTOR^{KinaseDomain} (AA1967-2549)	This paper	Addgene Cat# 120708
pLEX-FHH-MTOR^{HEAT} (AA1-409)	This paper	Addgene Cat# 120709
pLEX-FHH-MAPKAP1^{RBD} (AA279-353)	This paper	Addgene Cat# 120710

REAGENT or RESOURCE	SOURCE	IDENTIFIER
pLEX-FHH-MAPKAP1^{RBD}/Triple Mutant (AA279-353; K307A,K310A,R312L)	This paper	Addgene Cat# 120711
Software and Algorithms		
Preview	Protein Metrics	N/A
Byonic v2.6.49 or v2.14.27	Protein Metrics	N/A
Byologic	Protein Metrics	N/A
SAINT (Significance Analysis of INTeractome)	Choi et al., 2011	www.crapome.org
Cytoscape (v3.1.1)		www.cytoscape.org
MatLab	MathWorks	
STRING	Szklarczyk et al., 2015	string-db.org
Enrichr	Chen et al., 2013	http://amp.pharm.mssm.edu/Enrichr/
Bowtie	Langmead et al., 2009	http://bowtie-bio.sourceforge.net/index.shtml
MAGeCK	Li et al., 2014	https://sourceforge.net/projects/mageck/
Image Studio Lite	LI-COR	https://www.licor.com/bio/products/software/image_studio_lite/
GraphPad Prism 7.0d Software	GraphPad Software, Inc.	www.graphpad.com
Fiji (ImageJ)	Schindelin et al., 2012	fiji.sc
TopHat2	Kim et al., 2013	http://ccb.jhu.edu/software/tophat
CuffDiff2	Trapnell et al., 2013	https://github.com/cole-trapnell-lab/cufflinks
GSEA	Broad Institute	http://software.broadinstitute.org/gsea
LivingImage	Caliper LifeSciences	N/A
MO.Control Software v1.5.3	Nanotemper Technologies	N/A
MO.Affinity Analysis Software v2.2.7	Nanotemper Technologies	N/A
Other		
Immobilon-FL PVDF Membrane	Millipore Sigma	Cat# IPFL00010
Odyssey® Blocking Buffer (PBS)	LICOR	Cat# 927-4000
Monolith NT.115 Premium Capillaries	Nanotemper Technologies	Cat# MO-K025
Lysing Matrix D	MP Biomedicals	Cat# 116913500